

# 1 Global trends in marine nitrate N isotopes from observations and a neural network- 2 based climatology

3  
4 Patrick A. Rafter<sup>1</sup>, Aaron Bagnell<sup>2</sup>, Dario Marconi<sup>3</sup>, and Timothy DeVries<sup>2</sup>

5  
6 1: University of California, Irvine; 2 University of California, Santa Barbara; 3: Princeton  
7 University

## 8 9 **Abstract**

10 Nitrate is a critical ingredient for life in the ocean because, as the most abundant form of  
11 fixed nitrogen in the ocean, it is an essential nutrient for primary production. The  
12 availability of marine nitrate is principally determined by biological processes, each having  
13 a distinct influence on the N isotopic composition of nitrate (nitrate  $\delta^{15}\text{N}$ )—a property that  
14 informs much of our understanding of the marine N cycle as well as marine ecology,  
15 fisheries, and past ocean conditions. However, the sparse spatial distribution of nitrate  $\delta^{15}\text{N}$   
16 observations makes it difficult to apply this useful property in global studies, or to facilitate  
17 robust model-data comparisons. Here, we use a compilation of published nitrate  $\delta^{15}\text{N}$   
18 measurements ( $n = 12277$ ) and climatological maps of physical and biogeochemical tracers  
19 to create a surface-to-seafloor,  $1^\circ$  resolution map of nitrate  $\delta^{15}\text{N}$  using an Ensemble of  
20 Artificial Neural Networks (EANN). The strong correlation ( $R_2 > 0.87$ ) and small mean  
21 difference ( $<0.05\text{‰}$ ) between EANN-estimated and observed nitrate  $\delta^{15}\text{N}$  indicates that  
22 the EANN provides a good estimate of climatological nitrate  $\delta^{15}\text{N}$  without a significant bias.  
23 The magnitude of observation-model residuals is consistent with the magnitude of  
24 seasonal-decadal changes in observed nitrate  $\delta^{15}\text{N}$  that are not captured by our  
25 climatological model. As such, these observation-constrained results provide a globally-  
26 resolved map of mean nitrate  $\delta^{15}\text{N}$  for observational and modeling studies of marine  
27 biogeochemistry, paleoceanography, and marine ecology.

## 28 29 **1 Introduction**

30 In contrast to other marine nutrients (e.g., phosphate and silicate), the inventory of nitrate  
31 ( $\text{NO}_3^-$ ) is mediated by biological processes, where the main source is  $\text{N}_2$  fixation by  
32 diazotrophic phytoplankton and the main sink is denitrification (via a microbial  
33 consortium in oxygen deficient waters and sediments) (Codispoti and Christensen, 1985).  
34 Biological processes also determine the distribution of marine nitrate throughout the water  
35 column, with phytoplankton assimilating nitrate / lowering nitrate concentrations in the  
36 surface ocean and the microbially-mediated degradation of organic matter in the  
37 subsurface. (The latter involving the multi-step process of ammonification (organic matter  
38  $\rightarrow \text{NH}_4^+$ ) and nitrification ( $\text{NH}_4^+ \rightarrow \text{NO}_2^- \rightarrow \text{NO}_3^-$ )). By regulating the global inventory and  
39 distribution of marine nitrate, these N cycling processes control global net primary  
40 productivity, the transfer of nutrients to higher trophic levels such as fishes, and the  
41 strength of the ocean's biological carbon pump (Dugdale and Goering, 1967).

42  
43 Each of these biologically mediated N transformations affects the N isotopic composition of  
44 nitrate in unique ways (Figs 1A & 1B and see Section 2), adjusting the relative abundance  
45 of  $^{15}\text{N}$  and  $^{14}\text{N}$  in oceanic nitrate relative to the atmosphere.  $\delta^{15}\text{N} = (^{15}\text{N}/^{14}\text{N}_{\text{sample}} /$

46  $^{15}\text{N}/^{14}\text{N}$  standard) – 1), multiplied by 1000 to give units of per mil (‰); see (Sigman and  
47 Casciotti, 2001) for simplified equations from (Mariotti et al., 1981). Nitrate  $\delta^{15}\text{N}$   
48 measurements have become a powerful tool for understanding the ‘biogeochemical history’  
49 of marine nitrate, which includes nitrate assimilation by phytoplankton (Miyake and Wada,  
50 1967; Wada and Hattori, 1978), nitrogen fixation (Carpenter et al., 1997; Hoering and Ford,  
51 1960), denitrification (Liu, 1979), and nitrification (Casciotti et al., 2013). For example, the  
52 consumption of nitrate by denitrification (red line in Fig. 1A) has a larger impact on the  
53 residual nitrate  $\delta^{15}\text{N}$  than does partial nitrate assimilation by phytoplankton (yellow line in  
54 Fig. 1), and thus very high  $\delta^{15}\text{N}$  values serve as a fingerprint of denitrification. Nitrate  $\delta^{15}\text{N}$   
55 is also influenced by the addition of nitrate via remineralization of organic matter. The  
56 exact influence of remineralization depends on the isotopic composition of the organic  
57 matter, and could result in both higher or lower nitrate  $\delta^{15}\text{N}$  (Fig. 1A). Nitrate introduced  
58 into the water column by the remineralization of organic matter formed by  $\text{N}_2$ -fixing  
59 phytoplankton has an isotopic composition close to that of air (0-1‰), and serves to lower  
60 the mean ocean  $\delta^{15}\text{N}$  (Fig. 1B). On the other hand, organic matter formed from nitrate  
61 assimilation in regions where the plankton use most of the available nitrate can be  
62 isotopically heavy, and its remineralization will increase the  $\delta^{15}\text{N}$  of ambient nitrate (Fig.  
63 1B). The actual value of organic matter  $\delta^{15}\text{N}$  formed from nitrate assimilation is mostly  
64 determined by: (1) the  $\delta^{15}\text{N}$  of nitrate delivered to the euphotic zone (the subsurface  
65 source), which in turn is dependent on the degree of water-column denitrification and (2)  
66 the degree of nitrate consumption at the ocean surface, with heavier values associated with  
67 greater nitrate consumption (Fig. 1B). Accordingly, changes in organic matter  $\delta^{15}\text{N}$  (and  
68 therefore sediment  $\delta^{15}\text{N}$  used for paleoceanographic work) can reflect variability of the  
69 source nitrate  $\delta^{15}\text{N}$  and/or variability of the degree of nitrate consumption (e.g., see (Rafter  
70 and Charles, 2012)).

71  
72 Because of nitrate’s place at the base of the marine ecosystem, nitrate  $\delta^{15}\text{N}$  is also useful for  
73 understanding the lifecycles of higher trophic level organisms such as fish (Graham et al.,  
74 2007; Tawa et al., 2017) and fishery productivity (Finney et al., 2002, 2000). The  $\delta^{15}\text{N}$  of  
75 whole sediment and microfossils provides insight *by proxy* of past ocean nitrate  
76 transformations (Altabet and Francois, 1994a; Kienast et al., 2008; Ren et al., 2009;  
77 Robinson et al., 2004; Sigman et al., 1999b)—work that places important constraints on  
78 modern ocean N cycling (Altabet, 2007; Eugster et al., 2013; Ren et al., 2017). With an  
79 understanding of the N transformations described above and their influences on the N  
80 isotopic composition of nitrate, we can begin using nitrate  $\delta^{15}\text{N}$  measurements to trace the  
81 integrated biogeochemical history of marine nitrate. However, identifying basin- and  
82 global-scale trends in nitrate  $\delta^{15}\text{N}$  is challenged by the limited spatial extent of nitrate  $\delta^{15}\text{N}$   
83 observations (Fig. 2). Here, we compile a global database of nitrate  $\delta^{15}\text{N}$  measurements  
84 (Fig. 2) and use an Ensemble Artificial Neural Network (EANN) to produce a map of the  
85 global nitrate  $\delta^{15}\text{N}$  distribution at 1-degree spatial resolution. We find that the mapped  
86 nitrate  $\delta^{15}\text{N}$  climatology matches the observations well and should be a valuable tool for  
87 estimating mean conditions and for constraining predictive nitrate  $\delta^{15}\text{N}$  models (Somes et  
88 al., 2010; Yang and Gruber, 2016). Below we briefly discuss how the EANN was used to  
89 produce global maps of nitrate  $\delta^{15}\text{N}$  (Section 2), address the ability of the EANN to match

90 the measured  $\delta^{15}\text{N}$  (Section 3), and examine the EANN-mapped  $\delta^{15}\text{N}$  climatology and global  
91 compilation of nitrate  $\delta^{15}\text{N}$  in the context of published work (Section 4).

## 92 93 **2 Methods**

### 94 **2.1 Data Compilation**

95 Nitrate  $\delta^{15}\text{N}$  observations (Fig. 2; references in Table 3) were compiled from studies dating  
96 from 1975 (Cline and Kaplan, 1975) to 2018 (Fripiat et al., 2018), including data from the  
97 GEOTRACES Intermediate Data Product (Schlitzer et al., 2018). Whenever possible, the  
98 data was acquired via the original author, but in other cases the data was estimated from  
99 the publication directly. All observations were treated equally, although the failure to  
100 remove nitrite when using the “denitrifier method” may bias the nitrate  $\delta^{15}\text{N}$  to low values  
101 (Rafter et al., 2013). These measurements have been identified as “nitrate+nitrite” in the  
102 dataset to acknowledge this potential biasing, which predominantly affects observations in  
103 the upper 100 m (Kemeny et al., 2016; Rafter et al., 2013).

### 104 105 **2.2 Building the neural network model**

106 We utilize an ensemble of artificial neural networks (EANNs) to interpolate our global  
107 ocean nitrate  $\delta^{15}\text{N}$  database (Fig. 2), producing complete 3D maps of the data. By utilizing  
108 an artificial neural network (ANN), a machine learning approach that effectively identifies  
109 nonlinear relationships between a target variable (the isotopic dataset) and a set of input  
110 features (other available ocean datasets), we can fill holes in our data sampling coverage of  
111 nitrate  $\delta^{15}\text{N}$ .

#### 112 113 **2.2.1 Binning target variables (Step 1)**

114 We binned the nitrate  $\delta^{15}\text{N}$  observations (red symbols in Fig. 2) to the World Ocean Atlas  
115 2009 (WOA09) grid with a 1-degree spatial resolution and 33 vertical depth layers (0-5500  
116 m) (Garcia et al., 2010). When binning vertically, we use the depth layer whose value is  
117 closest to the observation’s sampling depth (e.g. the first depth layer has a value of 0 m, the  
118 second of 10 m, and the third of 20 m, so all nitrate isotopic data sampled between 0-5 m  
119 fall in the 0 m bin; between 5-15 m they fall in the 10 m bin, etc.). An observation with a  
120 sampling depth that lies right at the midpoint between depth layers is binned to the  
121 shallower layer. If more than one raw data point falls in a grid cell we take the average of all  
122 those points as the value for that grid cell. Certain whole ship tracks of nitrate  $\delta^{15}\text{N}$  data  
123 were withheld from binning to be used as an independent validation set (see section 2.2.4).

#### 124 125 **2.2.2 Obtaining input features (Step 2)**

126 Our input dataset contains a set of climatological values for physical and biogeochemical  
127 ocean parameters that form a non-linear relationship with the target data. We have six  
128 input features including objectively analyzed annual-mean fields for temperature, salinity,  
129 nitrate, oxygen, and phosphate taken from the WOA09  
130 (<https://www.nodc.noaa.gov/OC5/WOA09/woa09data.html>) at 1-degree resolution.  
131 Additionally, daily chlorophyll data from Modis Aqua for the period Jan-1-2003 through  
132 Dec-31-2012 is averaged and binned to the WOA09 grid (as described in Step 1) to produce  
133 an annual climatological field of chlorophyll values, which we then log transform to reduce  
134 their dynamic range.

135  
136 The choice of these specific input features was dictated by our desire to achieve the best  
137 possible R<sup>2</sup> value on our internal validation sets (Step 4). Additional inputs besides those  
138 we included, such as latitude, longitude, silicate, euphotic depth, or sampling depth either  
139 did not improve the R<sup>2</sup> value on the validation dataset or degraded it, indicating that they  
140 are not essential parameters for characterizing this system globally. By opting to use the  
141 set of input features that yielded the best results for the global oceans, we potentially  
142 overlooked combinations of inputs that perform better at regional scales. However, given  
143 the scarcity of δ<sup>15</sup>N data in some regions, it is not possible to ascribe the impact of a specific  
144 combination of input features versus the impact of available δ<sup>15</sup>N data, which may not be  
145 representative of the region's climatological state, to the relative model performance in  
146 these regions.

147

### 148 **2.2.3 Training the ANN (Step 3)**

149 The architecture of our ANN consists of a single hidden layer, containing 25 nodes, that  
150 connects the biological and physical input features (discussed in Step 2) to the target  
151 nitrate isotopic variable (as discussed in Step 1). The role of the hidden layer is to  
152 transform input features into new features contained in the nodes. These are given to the  
153 output layer to estimate the target variable, introducing nonlinearities via an activation  
154 function. The number of nodes in this hidden layer, as well as the number of input features,  
155 determines the number of adjustable weights (the free parameters) in the network.  
156 Because there is a danger of over-fitting the model, which occurs when the ANN is over-  
157 trained on a dataset so that it cannot generalize well when presented with new data, it is a  
158 good practice to have a large number of training data (we have 7170 binned data points)  
159 relative to the number of weights (we have 201 free parameters) (Weigend et al., 1990). To  
160 create a nonlinear system, an activation function transforms the product of the weights and  
161 input features and creates the values assigned to nodes in the hidden layer. These act as  
162 new features for estimating the target δ<sup>15</sup>N data. Our model utilizes the hyperbolic tangent  
163 as its activation function between the input and hidden layer as well as between the hidden  
164 and output layer due to its speed and general performance (Thimm and Fiesler, 1997).

165

166 The values of nodes in the hidden layer (H) can be defined as

167

$$H = a(I \cdot W_1 + b_1)$$

168

169 where H is an array containing the values of the hidden nodes, a is the activation function  
170 (here, the hyperbolic tangent), I is a 7170x6 array containing the values of the input  
171 features at the locations of the binned observations (there are 7170 binned observations  
172 and 6 input parameters), W<sub>1</sub> is a 6x25 array of weights that connect input features to  
173 hidden nodes, and b<sub>1</sub> is a 7170x25 array of weights (25 unique values repeated 7170 times)  
174 that connects a bias node to the hidden nodes. The factor of 25 represents the number of  
175 nodes in the hidden layer, chosen by experimentation to find the maximum number of  
176 effective parameters (Foresee and Hagan 1997), i.e. where adding new parameters no  
177 longer improves performance on an internal validation set (Step 4). The bias node acts as

178 an offset term, similar to a constant term in a linear function, and has a value that is always  
179 1.

180  
181 At the output layer, the network produces a prediction of the target nitrate isotopic data  
182 ( $\delta^{15}\text{N}_{\text{pred}}$ ). Similar to how nodes in the hidden layer are a function of the inputs and a set of  
183 weights,  $\delta^{15}\text{N}_{\text{pred}}$  is a function of the hidden nodes and an additional set of weights. The  
184 predicted values can be defined as

$$d^{15}\text{N}_{\text{pred}} = a(H \cdot W_2 + b_2)$$

186  
187 where H (size 7170x25) has been previously defined,  $W_2$  (size 25x1) is a matrix of weights  
188 that connect features in the hidden layer to nodes in the output layer, and  $b_2$  (size 7170x1)  
189 is an array of weights (all of the same value) that connects a bias node to the output layer.

190  
191 The ANN learns by comparing  $\delta^{15}\text{N}_{\text{pred}}$  to the actual  $\delta^{15}\text{N}$  data ( $\delta^{15}\text{N}_{\text{data}}$ ), attempting to  
192 minimize the value of the cost function

$$\text{cost} = \frac{\sum_{i=1}^n (d^{15}\text{N}_{\text{pred}}^i - d^{15}\text{N}_{\text{data}}^i)^2}{n}$$

194  
195 by iteratively adjusting the weights using the Levenberg-Marquardt algorithm (Marquardt,  
196 1963) as a way of propagating the errors between  $\delta^{15}\text{N}_{\text{pred}}$  and  $\delta^{15}\text{N}_{\text{data}}$  backwards through  
197 the network (Rumelhart et al., 1986).

#### 198 199 **2.2.4 Validating the ANN (Step 4)**

200 To ensure good generalization of the trained ANN, we randomly withhold 10% of the  $\delta^{15}\text{N}$   
201 data to be used as an internal validation set for each network. This is data that the network  
202 never sees, meaning it does not factor into the cost function, so it works as a test of the  
203 ANN's ability to generalize. This internal validation set acts as a gatekeeper to prevent poor  
204 models from being accepted into the ensemble of trained networks (see Step 5). A second,  
205 independent or 'external' validation set (blue symbols in Fig. 2), composed of complete ship  
206 transects from the high and low latitude ocean were omitted from binning in Step 1 and  
207 used to establish the performance of the entire ensemble. Our rationale for using complete  
208 ship transects is the following. If we randomly chose 10% of observations to perform an  
209 external validation, this dataset will be from the same cruises as the wider data. In other  
210 words, despite being randomly selected, the validating observational dataset will be highly  
211 correlated geographically. Contrast this with validating the EANN results with observations  
212 from whole research cruises in unique geographic regions—areas where the model has not  
213 "learned" anything about nitrate. We therefore argue that these observations from whole  
214 ship tracks therefore provide a more difficult test of the model.

#### 215 216 **2.2.5 Forming the Ensemble (Step 5)**

217 The ensemble is formed by repeating Steps 3 to 4 (using a different random 10% validation  
218 set) until we obtain 25 trained networks for the nitrate  $\delta^{15}\text{N}$  dataset. A network is admitted  
219 into the ensemble if it yields an  $R^2$  value greater than 0.81 on the validation dataset. Using

220 an EANN instead of any single network provides several advantages. For example, the  
221 random initialization of the weight values in each network as well as differences in the  
222 training and internal validation sets used across members make it possible for many  
223 different networks to achieve similar performance on their respective validation set while  
224 generalizing to areas with no data coverage differently. By performing this type of data  
225 subsampling and taking an ensemble average, similar to bootstrap aggregating (Breiman,  
226 1996) this approach on average improves the robustness of the generalization in areas  
227 without data coverage compared to a single randomly generated ensemble member.  
228 Compared to each of its members, our ensemble mean sees improved performance on all  
229 internal validation sets and has a higher  $R^2$  and lower root mean square error on the  
230 independent validation set compared to 19 of the 25 members. The range of values given  
231 by the ensemble also provides a measure of the uncertainty for our estimations of  $\delta^{15}\text{N}$ .

232

### 233 **3 Results**

#### 234 **3.1 Global nitrate $\delta^{15}\text{N}$ observations**

235 The global compilation of nitrate  $\delta^{15}\text{N}$  includes 1180 stations from all major ocean basins  
236 and some minor seas (Fig. 2) giving a total of 12277 nitrate  $\delta^{15}\text{N}$  measurements. Within  
237 this dataset, 1197 nitrate  $\delta^{15}\text{N}$  measurements were withheld from the EANN and used to  
238 validate the EANN results to ensure good extrapolation (the ‘external’ validation dataset;  
239 blue symbols in Fig. 2, see Section 2). With observations from the surface to as deep as  
240 6002 m (Rafter et al., 2012), we find that nitrate  $\delta^{15}\text{N}$  ranges from  $\approx 1\text{‰}$  in the North  
241 Atlantic (e.g., Marconi et al., (2015)) to 68.7‰ in the Eastern Tropical South Pacific  
242 (Bourbonnais et al., 2015). Nitrate  $\delta^{15}\text{N}$  of  $\approx 1\text{‰}$  was also irregularly observed in the  
243 shallow North and South Pacific (Liu et al., 1996; Yoshikawa et al., 2015). These latter  
244 observations were included in the training dataset, although we should note that the  
245 measurements using the ‘Devarda’s Alloy’ method (Liu et al., 1996) is thought to be biased  
246 low (Altabet and Francois, 2001). Similarly, the inclusion of nitrite for ‘denitrifier method’  
247 nitrate  $\delta^{15}\text{N}$  can bias the measurement to lower values (Kemeny et al., 2016; Rafter et al.,  
248 2013).

249

#### 250 **3.2 Marine nitrate $\delta^{15}\text{N}$ observations-model comparison**

251 The observed and EANN-predicted nitrate  $\delta^{15}\text{N}$  measurements are distributed around a 1:1  
252 line in Fig. 3A (all data), with considerably less scatter for the deeper values (data >1000 m;  
253 Fig. 3B). The correlation coefficient of determination for the observations versus the model  
254 nitrate  $\delta^{15}\text{N}$  gives an  $R^2=0.75$  for the raw / unbinned observations used to train the EANN  
255 and an  $R^2$  of 0.78 for the validation dataset. We can also examine the performance of the  
256 EANN with the nitrate  $\delta^{15}\text{N}$  “residual” or the difference between observed and modeled  
257  $\delta^{15}\text{N}$ , which indicates a mean residual or ‘mean bias’ value of  $-0.03\text{‰}$  for the entire dataset  
258 and  $+0.18\text{‰}$  for the validation dataset.

259

260 Examining the observation-EANN residuals via the Root Mean Square Error (RMSE), we  
261 find an RMSE of  $1.94\text{‰}$  for the data used to train the EANN and an RMSE of  $1.26\text{‰}$  for the  
262 external validation dataset. There is a clear relationship between RMSE and depth, with a  
263 significantly higher RMSE for the upper 500 m (Figs. 3C and 3D). Comparing these residual  
264 values with dissolved oxygen concentrations (color in Fig. 3C), we find that  $>2\text{‰}$  RMSE for

265 the surface is associated with high oxygen while  $>2.7\text{‰}$  RMSE at  $\approx 250$  m is associated with  
266 the lowest oxygen. Furthermore, the RMSE of the observation-EANN residuals differs  
267 between the datasets used to train the model (solid red line in Fig. 3D) and validate the  
268 model (dashed line in Fig. 3D).

269  
270 The RMSE patterns in Figs. 3C and 3D are to be expected given the natural variability in  
271 nitrate  $\delta^{15}\text{N}$  driven by assimilation in the upper ocean and denitrification in the shallow  
272 sub-surface—variability which is not captured by the climatological EANN. Rafter and  
273 Sigman, (2016), presented a 5-year time-series of nitrate  $\delta^{15}\text{N}$  from the eastern equatorial  
274 Pacific, which showed that variability of nitrate assimilation produces seasonal-to-  
275 interannual deviations of  $\delta^{15}\text{N}$  of  $\pm 2.5\text{‰}$ , which is similar to the magnitude of the RMSE in  
276 the surface ocean ( $2.2\text{‰}$ ). Although there are no nitrate  $\delta^{15}\text{N}$  time-series measurements  
277 from the subsurface Oxygen Deficient Zone (ODZ) waters where denitrification occurs,  
278 nitrate  $\delta^{15}\text{N}$  in ODZs presumably have similar seasonal-to-interannual (or longer timescale)  
279 variability due to changes in the rate and extent of water column denitrification (Deutsch et  
280 al., 2011; Yang et al., 2017). For example, a larger degree of nitrate undergoing water  
281 column denitrification would explain the extreme  $\delta^{15}\text{N}$  values at the bottom right of Fig.  
282 3A—observations that all come from the ODZ waters of the Eastern Tropical South Pacific  
283 (Bourbonnais et al., 2015; Casciotti et al., 2013; Rafter et al., 2012; Ryabenko et al., 2012).  
284 Some of these very high nitrate  $\delta^{15}\text{N}$  values are associated with nitrate concentrations  $<1$   
285  $\mu\text{mol kg}^{-1}$  (Bourbonnais et al., 2015), values much lower than within our climatology for the  
286 subsurface Eastern Tropical South Pacific. These values thus represent episodic  
287 denitrification events that the EANN will not be able to capture because it is trained on  
288 climatological data. In the deep ocean where temporal variability is smaller, the  
289 observation-EANN residuals of  $0.2\text{‰}$  are the same magnitude as the  $\delta^{15}\text{N}$  analytical errors,  
290 further emphasizing the ability of the model to match climatological average conditions.

#### 291 292 **4 Discussion**

293 The EANN's skillful estimate of climatological nitrate  $\delta^{15}\text{N}$  will be useful for studies of the  
294 marine nitrogen cycle. The zonal average view of EANN nitrate  $\delta^{15}\text{N}$  for each major ocean  
295 basin (Fig. 4) includes statistics comparing the observations versus EANN results above  
296 and below 1000 m. These region-specific statistics show a weaker correlation between  
297 EANN and observed nitrate  $\delta^{15}\text{N}$  in the deep Atlantic and Southern Ocean, despite low  
298 RMSE and negligible mean bias. This weak correlation likely derives from the limited  
299 variability of deep nitrate  $\delta^{15}\text{N}$  ( $\pm 0.1\text{‰}$ ) in these basins (see Fig. 5D).

300  
301 The nitrate  $\delta^{15}\text{N}$  sections in Fig. 4 show elevated values for the low latitude, upper  
302 mesopelagic Pacific (Fig. 4A) and Indian Oceans (Fig. 4D) where water column  
303 denitrification raises the residual nitrate  $\delta^{15}\text{N}$  (Fig. 1A). Viewing this elevated nitrate  $\delta^{15}\text{N}$   
304 at the 250 m depth horizon (Fig. 5) better reveals the spatial heterogeneity of the  
305 observations and EANN results. (It is because of this intra-basin heterogeneity, and the fact  
306 that many observations are biased towards the areas of denitrification, that we did not plot  
307 the observed nitrate  $\delta^{15}\text{N}$  within the zonally-averaged Fig. 4 views.) The EANN error for the  
308 Fig. 5 depth intervals (Figs. 5E-5H) is the standard deviation of the 25 ensemble members  
309 of the EANN and shows a decrease in ensemble variability with depth—a trend that is

310 consistent with the overall decrease in observed nitrate  $\delta^{15}\text{N}$  variability with depth (Figs. 4  
311 & 5).

312  
313 Below we inspect the observed and EANN-predicted nitrate  $\delta^{15}\text{N}$  and discuss the  
314 consistency of these results with our understanding of published work. This analysis begins  
315 with the spatial distribution of nitrate delivered to the upper ocean. We then discuss the  
316 impacts of upper ocean nitrate assimilation on organic matter  $\delta^{15}\text{N}$  and consider the  
317 influence of organic matter remineralization on sub-surface nitrate.

318

#### 319 **4.1 Subsurface and surface nitrate $\delta^{15}\text{N}$**

320 The nitrate  $\delta^{15}\text{N}$  distribution at 250 m depth (Fig. 5B) offers a view of nitrate at a depth  
321 that is deeper than source waters in many ocean regions (e.g., 100 to 150 m in the  
322 equatorial Pacific (Rafter and Sigman, 2016)), but is negligibly influenced by nitrate  
323 assimilation, and therefore provides a qualitative view of spatial trends in nitrate delivered  
324 to the surface ocean. Nitrate  $\delta^{15}\text{N}$  at this depth is highest in the North and South Eastern  
325 Tropical Pacific and Arabian Seas (Fig. 5B), due to the influence of water column  
326 denitrification in the ODZs in these regions (Altabet et al., 2012; Bourbonnais et al., 2015;  
327 Ryabenko et al., 2012), which preferentially uses the light isotope and leaves the residual  
328 nitrate enriched in  $^{15}\text{N}$ . A notable difference between the EANN and a previous  
329 biogeochemical model estimate of nitrate  $\delta^{15}\text{N}$  (Somes et al., 2010) is that the EANN  
330 correctly captures the higher nitrate  $\delta^{15}\text{N}$  in the Arabian Sea compared to the Bay of  
331 Bengal.

332

333 Lowest  $\delta^{15}\text{N}$  values of sub-surface nitrate are found in the Southern Ocean and in the North  
334 Atlantic. The North Atlantic subtropical gyre in particular has the lowest  $\delta^{15}\text{N}$  values in any  
335 basin (Fig. 5B; also see (Fawcett et al., 2011; Knapp et al., 2005, 2008)), which can be  
336 attributed to the remineralization of low- $\delta^{15}\text{N}$  organic matter originating from  $\text{N}_2$ -fixation,  
337 which produces organic matter with a  $\delta^{15}\text{N}$  between 0 and -1‰ (similar to atmospheric  $\text{N}_2$ ;  
338 see Fig. 1B (Carpenter et al., 1997; Hoering and Ford, 1960)). Prior work argues that this  
339 nitrate  $\delta^{15}\text{N}$  lowering requires the bulk of Atlantic  $\text{N}_2$ -fixation ( $\approx 90\%$ ) to occur in the  
340 tropics (Marconi et al., 2017) followed by the advection of remineralized nitrate to the  
341 North Atlantic. This contrasts with numerical models arguing for high  $\text{N}_2$ -fixation rates in  
342 the North Atlantic (Ko et al., 2018). Similar local minima of sub-surface  $\delta^{15}\text{N}$  appear in all  
343 the sub-tropical gyres (Fig. 5B), which is consistent with observations (Casciotti et al.,  
344 2008; Yoshikawa et al., 2015) and presumably indicates the importance of  $\text{N}_2$ -fixation in  
345 these regions (Ko et al., (2018) and others). The  $\text{N}_2$ -fixation  $\delta^{15}\text{N}$  signal in the Pacific Ocean  
346 is counteracted by the influence of water-column denitrification in that basin, which  
347 imparts a high  $\delta^{15}\text{N}$  signal, but a local minimum in  $\delta^{15}\text{N}$  can still be seen in the Pacific  
348 subtropical gyres (Fig. 4A).

349

350 Nitrate assimilation by phytoplankton in the upper ocean is influenced by both the  
351 subsurface source nitrate  $\delta^{15}\text{N}$  and the degree of nitrate assimilation (Miyake and Wada,  
352 1967; Wada and Hattori, 1978) (Fig. 1B). This gives the expectation that average nitrate  
353  $\delta^{15}\text{N}$  values for the upper 50 m (Fig. 5A) will be consistently higher than those at 250 m  
354 (Fig. 5B). However, the highest values in the upper 50 m are not found above the ODZ



355 regions, but are on the edges of high nitrate concentration upwelling zones in the Southern  
356 Ocean, equatorial Pacific, and subarctic gyres (contours in Fig. 2). Circulation in these ‘edge’  
357 regions allows for nitrate to be advected along the surface, lengthening its time in the  
358 surface ocean and allowing more utilization to elevate the residual nitrate  $\delta^{15}\text{N}$  pool. In  
359 other words, the degree of nitrate utilization appears to play a more important role in  
360 determining surface nitrate  $\delta^{15}\text{N}$  than the initial value. (This is not the case for the organic  
361 matter  $\delta^{15}\text{N}$  produced from this nitrate, which will be discussed more below.)  
362

363 Despite our expectation of higher nitrate  $\delta^{15}\text{N}$  in the upper 50 m versus 250 m (Figs. 5A vs.  
364 5B), we identify two types of regions where this difference is negative (Fig. 6): above ODZ  
365 waters and in subtropical gyres. The explanation for the negative values above the ODZ  
366 regions is that the nitrate  $\delta^{15}\text{N}$  at 250 m must be much higher than the nitrate  $\delta^{15}\text{N}$   
367 upwelled to the surface. This is consistent with elevated ODZ nitrate  $\delta^{15}\text{N}$  having an  
368 indirect path to waters outside of ODZ regions (Peters et al., 2017; Rafter et al., 2013). The  
369 subtropical gyres also have modeled nitrate  $\delta^{15}\text{N}$  in the upper 50 m that is less than 250 m,  
370 but this finding is difficult to test with observations because of low nitrate concentrations.  
371 That said, the model predicts a lower nitrate  $\delta^{15}\text{N}$  in the upper ocean relative to that at 250  
372 m, which is consistent with  $\text{N}_2$ -fixation in these regions.  
373

374 Our discussion above highlights the difficulty of distinguishing between the competing  
375 influences of the subsurface source nitrate  $\delta^{15}\text{N}$  and the degree of nitrate utilization on  
376 residual nitrate  $\delta^{15}\text{N}$ . Clearly a static depth does not reflect the subsurface source of nitrate  
377 delivered to the surface and a more robust method for estimating this subsurface source  
378 needs to be developed. However, some generalizations can be made regarding the organic  
379 matter  $\delta^{15}\text{N}$  produced in these regions and its potential influence (via remineralization) on  
380 subsurface nitrate throughout the water column via the export and remineralization of  
381 organic matter (Sigman et al., 2009a). For example, a local minimum in  $\delta^{15}\text{N}$  is visible at  
382 250 m depth in the Eastern Equatorial Pacific (Fig. 5B; also discussed in several studies  
383 (Rafter et al., 2012; Rafter and Sigman, 2016)) is caused by the remineralization of organic  
384 matter with a low  $\delta^{15}\text{N}$  due to partial nitrate consumption at the surface. Below we discuss  
385 these and other influences on intermediate-depth nitrate  $\delta^{15}\text{N}$ .  
386

#### 387 **4.2 Intermediate-depth nitrate $\delta^{15}\text{N}$ variability**

388 Waters at “intermediate” depths (here shown as the 750 m surface in Fig. 5C) are important  
389 because they are part of a large-scale circulation that initially upwells in the Southern  
390 Ocean and ultimately resupplies nutrients to the low latitude thermocline (Palter et al.,  
391 2010; Sarmiento et al., 2004; Toggweiler et al., 1991; Toggweiler and Carson, 1995). Within  
392 the context of this overturning, the nitrate upwelling in the Southern Ocean is initially  
393  $\approx 5\text{‰}$  (Figs. 4C & 5C) and the  $\delta^{15}\text{N}$  is elevated  $\approx 2\text{‰}$  by partial nitrate assimilation in  
394 surface waters as they are advected equatorward (see Figs. 5A and 6). Deep wintertime  
395 mixing in the Subantarctic Pacific converts these surface waters into mode and  
396 intermediate waters (Herraiz-Borreguero and Rintoul, 2011), introducing nitrate with a  
397 “pre-formed”  $\delta^{15}\text{N}$  of  $\approx 6\text{‰}$  into the intermediate-depth South Pacific and South Atlantic  
398 (Rafter et al., 2012, 2013; Tuerena et al., 2015) at depths between  $\approx 600$ -1200 m. The

399 penetration of this pre-formed signal (nitrate  $\geq 6\text{‰}$ ) into the interior can be clearly seen in  
400 the Atlantic Ocean between  $\approx 40^\circ\text{S}$  to  $20^\circ\text{N}$  (Fig. 4B).

401  
402 The same signal is carried with Southern Ocean mode and intermediate waters into the  
403 Pacific basin as far as the tropics (Lehmann et al., 2018; Rafter et al., 2013), although it is  
404 difficult to distinguish in the model results against the higher background  $\delta^{15}\text{N}$  in this  
405 basins (Figs. 4A, 4D, 5C). The same process presumably introduces elevated nitrate  $\delta^{15}\text{N}$  to  
406 the Indian Ocean, which has similar values at this depth. Nitrate  $\delta^{15}\text{N}$  increases from the  
407 Southern Ocean toward the equator in the Pacific and Indian Oceans, but not in the Atlantic  
408 (Fig. 5C). Organic matter has a lower  $\delta^{15}\text{N}$  in the Atlantic than in the Pacific and Indian  
409 because of a lack of water-column denitrification supplying high- $\delta^{15}\text{N}$  water to the surface,  
410 and because of the high rates of  $\text{N}_2$ -fixation which supply isotopically light N to organic  
411 matter (Marconi et al., 2017; Tuerena et al., 2015). This contrast in intermediate-depth  
412 nitrate  $\delta^{15}\text{N}$  can be traced to the lower  $\delta^{15}\text{N}$  of organic matter remineralized in this  
413 region—an explanation that is also consistent with enhanced  $\text{N}_2$  fixation in the tropical  
414 Atlantic (Marconi et al., 2017). The increase in intermediate-depth nitrate  $\delta^{15}\text{N}$  from the  
415 Subantarctic to the tropical Pacific appears to result from the remineralization of organic  
416 matter with a  $\delta^{15}\text{N}$  elevated by high source nitrate  $\delta^{15}\text{N}$  (near the ODZ) or extreme  
417 elevation of residual nitrate  $\delta^{15}\text{N}$  (advected along the surface away from the equator; see  
418 high surface nitrate  $\delta^{15}\text{N}$  in Fig. 5A). Previous work suggests that direct mixing with  
419 denitrified waters represents only a small fraction of the change from the pre-formed high  
420 latitude value ( $\approx 6\text{‰}$ ) to tropical nitrate  $\delta^{15}\text{N}$  of  $\approx 7\text{‰}$  (Peters et al., 2017; Rafter et al.,  
421 2012, 2013).

422  
423 The South Indian Ocean is one region particularly devoid of published nitrate  $\delta^{15}\text{N}$   
424 observations (Fig. 2), but the EANN makes specific predictions about its distribution. For  
425 example, the modeled nitrate  $\delta^{15}\text{N}$  predicts that intermediate-depth Indian Ocean nitrate is  
426 similarly elevated in  $\delta^{15}\text{N}$  to the intermediate-depth South Pacific (Fig. 5C). Considering  
427 that both intermediate-depth water masses are formed from Southern Ocean surface  
428 waters, it is reasonable to propose that nitrate  $\delta^{15}\text{N}$  are similarly elevated by partial nitrate  
429 consumption. The EANN therefore provides testable predictions for nitrate  $\delta^{15}\text{N}$   
430 observations throughout the Indian Ocean.

#### 431 432 **4.4 Deep-sea nitrate $\delta^{15}\text{N}$ trends**

433 Our discussion above suggests that the basin-scale balance of  $\text{N}_2$ -fixation and water-column  
434 denitrification is a major contributor to inter-basin nitrate  $\delta^{15}\text{N}$  gradients in the upper  
435 ocean, lowering values in the Atlantic Oceans compared to the Pacific and Indian Oceans.  
436 Averaging EANN nitrate  $\delta^{15}\text{N}$  with depth for each ocean basin (Fig. 7), we find that these  
437 basin-scale nitrate  $\delta^{15}\text{N}$  differences also persist into the deep-sea (here defined as  $\geq 3000$  m  
438 and below). (Note that the inter-basin EANN nitrate  $\delta^{15}\text{N}$  gradients in Fig. 7 are smaller  
439 than the corresponding inter-basin gradients in observed  $\delta^{15}\text{N}$ , because the observations  
440 are spatially biased towards areas of water column denitrification in the Pacific and Indian  
441 Oceans (see Fig. 2).)

442

443 The remineralization of organic matter is one process that can—and has been used to—  
444 explain both the elevation of deep Pacific nitrate  $\delta^{15}\text{N}$  (Peters et al., 2017; Rafter et al.,  
445 2013; Sigman et al., 2009a)(Peters et al., 2017; Rafter et al., 2013; Sigman et al., 2009) and  
446 lowering of deep Atlantic nitrate  $\delta^{15}\text{N}$  (Knapp et al., 2008; Marconi et al., 2017; Tuerena et  
447 al., 2015) relative to the deep ocean mean. Here we provide two additional pieces of  
448 evidence that argue for the remineralization of organic matter as the key driver of these  
449 deep-sea nitrate  $\delta^{15}\text{N}$  differences. Our first piece of evidence is that the average subsurface  
450 source of nitrate to the Pacific and Indian Ocean surface has a significantly higher  $\delta^{15}\text{N}$  (by  
451 2‰ at the 250 m depth surface) than the Atlantic and Southern Oceans (Figs. 5B and 7).  
452 Nitrate  $\delta^{15}\text{N}$  at 250 m is an admittedly imprecise estimate for the nitrate upwelled to the  
453 surface, but even a slight elevation in Pacific source nitrate  $\delta^{15}\text{N}$  and near complete nitrate  
454 utilization at the surface will translate into higher sinking organic matter  $\delta^{15}\text{N}$  (i.e., see Fig.  
455 1B).

456  
457 Our second piece of evidence that the export and remineralization of organic matter drives  
458 the inter-basin differences in deep nitrate  $\delta^{15}\text{N}$  comes from sediment trap measurements.  
459 Averaging published sediment trap organic matter  $\delta^{15}\text{N}$  from the subtropical and tropical  
460 Pacific gives a value of  $8.5 \pm 2.9\text{‰}$  (Knapp et al., 2016; Robinson et al., 2012), which is  
461 significantly higher than measured in traps from the Atlantic ( $4.5 \pm 1.5\text{‰}$ ) (Freudenthal et  
462 al., 2001; Holmes et al., 2002; Lavik, 2000; Thunell et al., 2004). Given observed Southern  
463 Ocean nitrate characteristics (Rafter et al., 2013), we estimate an even lower typical sinking  
464 organic matter  $\delta^{15}\text{N}$  of  $+1.5\text{‰}$  for this region, which assumes initial nitrate values equal the  
465 Upper Circumpolar Deep Water and final values from the Open Antarctic Zone. This value is  
466 consistent with annually-averaged sinking organic matter  $\delta^{15}\text{N}$  of  $\approx 0.9$  to  $1.6\text{‰}$  (Lourey et  
467 al., 2003), although published results from the iron-fertilized Kerguelen Plateau region are  
468 predictably higher (Trull et al., 2008). The much lower Southern Ocean sinking organic  
469 matter  $\delta^{15}\text{N}$  is consistent with partial consumption of nitrate at the surface (see Fig. 1B)  
470 and the entrainment of this nitrate in equatorward-moving intermediate waters acts to  
471 export nitrate with elevated  $\delta^{15}\text{N}$  to intermediate waters throughout the Southern  
472 Hemisphere (see discussion above). Based on this evidence, it appears that global patterns  
473 of sinking organic matter  $\delta^{15}\text{N}$  are consistent with the remineralization of this organic  
474 matter driving subtle, but significant differences in deep-sea nitrate  $\delta^{15}\text{N}$ .

475  
476 An alternative explanation for the deep-sea nitrate  $\delta^{15}\text{N}$  differences in Fig. 7 is that they  
477 reflect the lateral (along isopycnal) advection of elevated nitrate  $\delta^{15}\text{N}$  from ODZ regions.  
478 However, we can easily dismiss this explanation by looking at the meridional trends in  
479 deep-sea nitrate  $\delta^{15}\text{N}$ —following the deep waters from their entrance in the south and  
480 movement northward. What we find is that deep EANN nitrate  $\delta^{15}\text{N}$  (Fig. 5D) is lowest in  
481 the Southern Ocean and increases equatorward in the Pacific (Table 1). Average deep-sea  
482 nitrate  $\delta^{15}\text{N}$  for the global ocean is  $5.0 \pm 0.3\text{‰}$  (similar to suggested by Sigman et al., 1999),  
483 but average observed nitrate  $\delta^{15}\text{N}$  below 3000 m increases from  $4.7 \pm 0.1\text{‰}$  in the Pacific  
484 sector of the Southern Ocean to  $4.9 \pm 0.2\text{‰}$  in the deep South Pacific,  $5.4 \pm 0.2\text{‰}$  in the deep  
485 tropical Pacific, and  $5.2 \pm 0.2\text{‰}$  in the deep North Pacific (Table 1). This is consistent with  
486 the known increase in nitrate concentrations and lowering of deep oxygen concentrations  
487 from the deep South to Tropical and North Pacific (e.g., see Fig. 4E in (Rafter et al., 2013)).

488 This contrasts with no significant change in deep Atlantic nitrate  $\delta^{15}\text{N}$ , despite the export of  
489 slightly elevated nitrate  $\delta^{15}\text{N}$  into intermediate-depth Atlantic (see above and (Tuerena et  
490 al., 2015)) and the introduction of a different deep water mass (North Atlantic Deep Water)  
491 in the North Atlantic. The distribution of deep Pacific nitrate  $\delta^{15}\text{N}$  is coherent with elevated  
492 organic matter  $\delta^{15}\text{N}$  being produced and exported from the lower latitude surface and  
493 remineralized at depth. In other words, inter-basin differences sinking organic matter  $\delta^{15}\text{N}$   
494 best explains the inter-basin differences in deep EANN and observed nitrate  $\delta^{15}\text{N}$ .  
495 Diapycnal mixing from the low latitude Pacific ODZ regions may also play a role in the  
496 south-to-north elevation of deep Pacific nitrate  $\delta^{15}\text{N}$ , but we cannot quantify the magnitude  
497 of that influence without a circulation model. Future work should look into this issue.  
498

## 499 **5 Conclusions**

500 We find that an Ensemble of Artificial Neural Networks (EANN) can be trained on  
501 climatological distributions of physical and biogeochemical tracers to reproduce a global  
502 database of nitrate  $\delta^{15}\text{N}$  observations (Fig. 2) with good fidelity (Fig. 3). We used the EANN  
503 to produce global climatological maps of nitrate  $\delta^{15}\text{N}$  at a 1 degree-resolution from the  
504 surface to the seafloor. These results help identify spatial patterns (Figs. 4-6) and quantify  
505 regional and basin-average oceanic values of nitrate  $\delta^{15}\text{N}$  (Fig. 7). Major differences  
506 between the observed and EANN-predicted nitrate  $\delta^{15}\text{N}$  appear to be caused by temporal  
507 variability of nitrate  $\delta^{15}\text{N}$  in the upper ocean and in ODZs associated with variable nitrate  
508 uptake and denitrification rates. Additional measurements of nitrate  $\delta^{15}\text{N}$  will help to  
509 develop seasonally-resolved maps that can improve upon the climatological mean map  
510 provided here.  
511

512 Acknowledgments: M. Altabet, K. Casciotti, A. Santoro, B. Pasquier, J. J. Becker, two  
513 anonymous reviewers and M. Kienast, as well as J. Granger and D. M. Sigman for (at-the-  
514 time) unpublished data. A complete list of references can be found in the Appendix. The  
515 compiled data set and data product is available in several online databases (BCO-DMO.org,  
516 pangaea.de, and webodv.awi.de). Many figures were made using Ocean Data View software  
517 (Schlitzer, 2002). Custom made color palettes and are available via [www.prafter.com](http://www.prafter.com).  
518

519 **References**

- 520 Altabet, M. A.: Constraints on oceanic N balance/imbalance from sedimentary N-15 records,  
521 *Biogeosciences*, 4(1), 75–86, 2007.
- 522 Altabet, M. A. and Francois, R.: Sedimentary nitrogen isotopic ratio as a recorder for surface  
523 ocean nitrate utilization, *Glob. Biogeochem. Cycles*, 8(1), 103–116, 1994a.
- 524 Altabet, M. A. and Francois, R.: The use of nitrogen isotopic ratio for reconstruction of past  
525 changes in surface ocean nutrient utilization, in *Carbon Cycling in the Glacial Ocean:  
526 Constraints on the Ocean's Role in Global Change*, vol. 117, pp. 281–306, Springer-Verlag  
527 Berlin Heidelberg, 1994b.
- 528 Altabet, M. A. and Francois, R.: Nitrogen isotope biogeochemistry of the antarctic polar  
529 frontal zone at 170 degrees W, *Deep-Sea Res. Part II-Top. Stud. Oceanogr.*, 48(19–20),  
530 4247–4273, 2001.
- 531 Altabet, M. A., Murray, D. W. and Prell, W. L.: Climatically linked oscillations in Arabian Sea  
532 denitrification over the past 1m.y.: Implications for the marine N cycle, *Paleoceanography*,  
533 14(6), 732–743, 1999.
- 534 Altabet, M. A., Ryabenko, E., Stramma, L., Wallace, D. W. R., Frank, M., Grasse, P. and Lavik,  
535 G.: An eddy-stimulated hotspot for fixed nitrogen-loss from the Peru oxygen minimum  
536 zone, *Biogeosciences*, 9(12), 4897–4908, doi:10.5194/bg-9-4897-2012, 2012.
- 537 Altabet, M. A., Pilskaln, C. .. Thunell, R. .. Pride, C. .. Sigman, D. .. Chavez, F. .. Francois, R.: The  
538 nitrogen isotope biogeochemistry of sinking particles from the margin of the Eastern North  
539 Pacific, *Deep-Sea Res. Part -Oceanogr. Res. Pap.*, 46(4), 655–679, 1999.
- 540 Bourbonnais, A., Lehmann, M. F., Waniek, J. J. and Schulz-Bull, D. E.: Nitrate isotope  
541 anomalies reflect N<sub>2</sub> fixation in the Azores Front region (subtropical NE Atlantic), *J.*  
542 *Geophys. Res.*, 114(C3), doi:10.1029/2007JC004617, 2009.
- 543 Bourbonnais, A., Altabet, M. A., Charoenpong, C. N., Larkum, J., Hu, H., Bange, H. W. and  
544 Stramma, L.: N-loss isotope effects in the Peru oxygen minimum zone studied using a  
545 mesoscale eddy as a natural tracer experiment, *Glob. Biogeochem. Cycles*, 29(6), 793–811,  
546 doi:10.1002/2014GB005001, 2015.
- 547 Brandes, J. A., Devol, A. H., Yoshinari, T., Jayakumar, D. A. and Naqvi, S. W. A.: Isotopic  
548 composition of nitrate in the central Arabian Sea and eastern tropical North Pacific: A  
549 tracer for mixing and nitrogen cycles, *Limnol. Oceanogr.*, 43(7), 1680–1689, 1998.
- 550 Breiman, L.: Bagging predictors, *Mach. Learn.*, 24(2), 123–140, doi:10.1007/BF00058655,  
551 1996.
- 552 Carpenter, E. J., Harvey, H. R., Fry, B. and Capone, D. G.: Biogeochemical tracers of the  
553 marine cyanobacterium *Trichodesmium*, *Deep-Sea Res. Part -Oceanogr. Res. Pap.*, 44(1),  
554 27–38, doi:10.1016/s0967-0637(96)00091-x, 1997.

- 555 Casciotti, K. L. and McIlvin, M. R.: Isotopic analyses of nitrate and nitrite from reference  
556 mixtures and application to Eastern Tropical North Pacific waters, *Mar. Chem.*, 107(2),  
557 184–201, doi:10.1016/j.marchem.2007.06.021, 2007.
- 558 Casciotti, K. L., Trull, T. W., Glover, D. M. and Davies, D.: Constraints on nitrogen cycling at  
559 the subtropical North Pacific Station ALOHA from isotopic measurements of nitrate and  
560 particulate nitrogen, *Deep-Sea Res. Part II-Top. Stud. Oceanogr.*, 55(14–15), 1661–1672,  
561 doi:10.1016/j.dsr2.2008.04.017, 2008.
- 562 Casciotti, K. L., Buchwald, C. and McIlvin, M.: Implications of nitrate and nitrite isotopic  
563 measurements for the mechanisms of nitrogen cycling in the Peru oxygen deficient zone,  
564 *Deep Sea Res. Part Oceanogr. Res. Pap.*, 80, 78–93, doi:10.1016/j.dsr.2013.05.017, 2013.
- 565 Cline, J. D. and Kaplan, I. R.: Isotopic fractionation of dissolved nitrate during denitrification  
566 in the eastern tropical North Pacific Ocean, *Mar. Chem.*, 3(4), 271–299, doi:10.1016/0304-  
567 4203(75)90009-2, 1975.
- 568 Codispoti, L. . and Christensen, J. .: Nitrification, denitrification and nitrous oxide cycling in  
569 the eastern tropical South Pacific ocean, *Mar. Chem.*, 16(4), 277–300, doi:10.1016/0304-  
570 4203(85)90051-9, 1985.
- 571 De Pol-Holz, R., Robinson, R. S., Hebbeln, D., Sigman, D. M. and Ulloa, O.: Controls on  
572 sedimentary nitrogen isotopes along the Chile margin, *Deep-Sea Res. Part II-Top. Stud.*  
573 *Oceanogr.*, 56(16), 1100–1112, doi:10.1016/j.dsr2.2008.09.014, 2009.
- 574 Dehairs, F., Fripiat, F., Cavagna, A.-J., Trull, T. W., Fernandez, C., Davies, D., Roukaerts, A.,  
575 Fonseca Batista, D., Planchon, F. and Elskens, M.: Nitrogen cycling in the Southern Ocean  
576 Kerguelen Plateau area: evidence for significant surface nitrification from nitrate isotopic  
577 compositions, *Biogeosciences*, 12(5), 1459–1482, doi:10.5194/bg-12-1459-2015, 2015.
- 578 Deutsch, C., Brix, H., Ito, T., Frenzel, H. and Thompson, L.: Climate-Forced Variability of  
579 Ocean Hypoxia, *Science*, 333(6040), 336–339, doi:10.1126/science.1202422, 2011.
- 580 DeVries, T., Deutsch, C., Rafter, P. A. and Primeau, F.: Marine denitrification rates  
581 determined from a global 3-dimensional inverse model, *Biogeosciences Discuss.*, 9(10),  
582 14013–14052, doi:10.5194/bgd-9-14013-2012, 2012.
- 583 DiFiore, P. J., Sigman, D. M., Trull, T. W., Lourey, M. J., Karsh, K., Cane, G. and Ho, R.: Nitrogen  
584 isotope constraints on subantarctic biogeochemistry, *J. Geophys. Res.-Oceans*, 111(C8),  
585 doi:10.1029/2005jc003216, 2006.
- 586 Dugdale, R. C. and Goering, J. J.: Uptake of new and regenerated forms of nitrogen in  
587 primary production, *Limnol. Oceanogr.*, 12(2), 196–206, 1967.
- 588 Eugster, O., Gruber, N., Deutsch, C., Jaccard, S. L. and Payne, M. R.: The dynamics of the  
589 marine nitrogen cycle across the last deglaciation, *Paleoceanography*, 28(1), 116–129,  
590 doi:10.1002/palo.20020, 2013.

- 591 Fawcett, S. E., Lomas, M., Casey, J. R., Ward, B. B. and Sigman, D. M.: Assimilation of upwelled  
592 nitrate by small eukaryotes in the Sargasso Sea, *Nat. Geosci.*, 4(10), 717–722,  
593 doi:10.1038/ngeo1265, 2011.
- 594 Finney, B. P., Gregory-Eaves, I., Douglas, M. S. V. and Smol, J. P.: Fisheries productivity in the  
595 northeastern Pacific Ocean over the past 2,200 years, *Nature*, 416(6882), 729–733,  
596 doi:10.1038/416729a, 2002.
- 597 Finney, B. P. et al.: Impacts of Climatic Change and Fishing on Pacific Salmon Abundance  
598 Over the Past 300 Years, *Science*, 290, 795-799., 2000.
- 599 Freudenthal, T., Neuer, S., Meggers, H., Davenport, R. and Wefer, G.: Influence of lateral  
600 particle advection and organic matter degradation on sediment accumulation and stable  
601 nitrogen isotope ratios along a productivity gradient in the Canary Islands region, *Mar.*  
602 *Geol.*, 17, 2001.
- 603 Fripiat, F., Declercq, M., Sapart, C. J., Anderson, L. G., Bruechert, V., Deman, F., Fonseca-  
604 Batista, D., Humborg, C., Roukaerts, A., Semiletov, I. P. and Dehairs, F.: Influence of the  
605 bordering shelves on nutrient distribution in the Arctic halocline inferred from water  
606 column nitrate isotopes, *Limnol. Oceanogr.*, 63(5), 2018.
- 607 Galbraith, E. D.: Interactions between climate and the marine nitrogen cycle on glacial-  
608 interglacial timescales, University of British Columbia, Vancouver., 2007.
- 609 Garcia, H. E., Locarnini, T. P., Boyer, T. P., Antonov, J. I., Zweng, M. M., Baranova, O. K. and  
610 Johnson, D. R.: Volume 4: Nutrients (phosphate, nitrate, and silicate), in *World Ocean Atlas*  
611 2009, pp. 1–44, U.S. Government Printing Office., 2010.
- 612 Gaye, B., Nagel, B., Dähnke, K., Rixen, T. and Emeis, K.-C.: Evidence of parallel denitrification  
613 and nitrite oxidation in the ODZ of the Arabian Sea from paired stable isotopes of nitrate  
614 and nitrite, *Glob. Biogeochem. Cycles*, 27(4), 1059–1071, doi:10.1002/2011GB004115,  
615 2013.
- 616 Graham, B. S., Grubbs, D., Holland, K. and Popp, B. N.: A rapid ontogenetic shift in the diet of  
617 juvenile yellowfin tuna from Hawaii, *Mar. Biol.*, 150(4), 647–658, doi:10.1007/s00227-006-  
618 0360-y, 2007.
- 619 Granger, J., Prokopenko, M. G., Sigman, D. M., Mordy, C. W., Morse, Z. M., Morales, L. V.,  
620 Sambrotto, R. N. and Plessen, B.: Coupled nitrification-denitrification in sediment of the  
621 eastern Bering Sea shelf leads to (15)N enrichment of fixed N in shelf waters, *J. Geophys.*  
622 *Res.-Oceans*, 116, doi:10.1029/2010jc006751, 2011.
- 623 Granger, J., Prokopenko, M. G., Mordy, C. W. and Sigman, D. M.: The proportion of  
624 remineralized nitrate on the ice-covered eastern Bering Sea shelf evidenced from the  
625 oxygen isotope ratio of nitrate, *Glob. Biogeochem. Cycles*, 27(3), 962–971,  
626 doi:10.1002/gbc.20075, 2013.

- 627 Herraiz-Borreguero, L. and Rintoul, S. R.: Subantarctic mode water: distribution and  
628 circulation, *Ocean Dyn.*, 61(1), 103–126, doi:10.1007/s10236-010-0352-9, 2011.
- 629 Hoering, T. C. and Ford, H. T.: The isotope effect in the fixation of nitrogen by azotobacter, *J.*  
630 *Am. Chem. Soc.*, 82(2), 376–378, doi:10.1021/ja01487a031, 1960.
- 631 Holmes, E., Lavik, G., Fischer, G., Segl, M., Ruhland, G. and Wefer, G.: Seasonal variability of  
632  $\delta^{15}\text{N}$  in sinking particles in the Benguela upwelling region, , 18, 2002.
- 633 Karsh, K. L., Trull, T. W., Lourey, A. J. and Sigman, D. M.: Relationship of nitrogen isotope  
634 fractionation to phytoplankton size and iron availability during the Southern Ocean Iron  
635 RElease Experiment (SOIREE), *Limnol. Oceanogr.*, 48(3), 1058–1068, 2003.
- 636 Kemeny, P. C., Weigand, M. A., Zhang, R., Carter, B. R., Karsh, K. L., Fawcett, S. E. and Sigman,  
637 D. M.: Enzyme-level interconversion of nitrate and nitrite in the fall mixed layer of the  
638 Antarctic Ocean: Antarctic Fall Nitrate Isotopes, *Glob. Biogeochem. Cycles*, 30(7), 1069–  
639 1085, doi:10.1002/2015GB005350, 2016.
- 640 Kienast, M., Lehmann, M. F., Timmermann, A., Galbraith, E., Bolliet, T., Holbourn, A.,  
641 Normandeau, C. and Laj, C.: A mid-Holocene transition in the nitrogen dynamics of the  
642 western equatorial Pacific: Evidence of a deepening thermocline?, *Geophys. Res. Lett.*,  
643 35(23), doi:10.1029/2008gl035464, 2008.
- 644 Knapp, A. N., Sigman, D. M. and Lipschultz, F.: N isotopic composition of dissolved organic  
645 nitrogen and nitrate at the Bermuda Atlantic time-series study site, *Glob. Biogeochem.*  
646 *Cycles*, 19(1), doi:10.1029/2004gb002320, 2005.
- 647 Knapp, A. N., DiFiore, P. J., Deutsch, C., Sigman, D. M. and Lipschultz, F.: Nitrate isotopic  
648 composition between Bermuda and Puerto Rico: Implications for  $\text{N}(2)$  fixation in the  
649 Atlantic Ocean, *Glob. Biogeochem. Cycles*, 22(3), doi:10.1029/2007gb003107, 2008.
- 650 Knapp, A. N., Sigman, D. M., Lipschultz, F., Kustka, A. B. and Capone, D. G.: Interbasin isotopic  
651 correspondence between upper-ocean bulk DON and subsurface nitrate and its  
652 implications for marine nitrogen cycling, *Glob. Biogeochem. Cycles*, 25,  
653 doi:10.1029/2010gb003878, 2011.
- 654 Knapp, A. N., Casciotti, K. L., Berelson, W. M., Prokopenko, M. G. and Capone, D. G.: Low rates  
655 of nitrogen fixation in eastern tropical South Pacific surface waters, *Proc. Natl. Acad. Sci.*,  
656 113(16), 4398–4403, doi:10.1073/pnas.1515641113, 2016.
- 657 Ko, Y. H., Lee, K., Takahashi, T., Karl, D. M., Kang, S.-H. and Lee, E.: Carbon-Based Estimate of  
658 Nitrogen Fixation-Derived Net Community Production in N-Depleted Ocean Gyres, *Glob.*  
659 *Biogeochem. Cycles*, doi:10.1029/2017GB005634, 2018.
- 660 Lavik, G.: Nitrogen isotopes of sinking matter and sediments in the South Atlantic,  
661 Universität Bremen, Bremen, Deutschland., 2000.



- 662 Lehmann, M. F., Sigman, D. M., McCorkle, D. C., Brunelle, B. G., Hoffmann, S., Kienast, M.,  
663 Cane, G. and Clement, J.: Origin of the deep Bering Sea nitrate deficit: Constraints from the  
664 nitrogen and oxygen isotopic composition of water column nitrate and benthic nitrate  
665 fluxes, *Glob. Biogeochem. Cycles*, 19(4), doi:10.1029/2005gb002508, 2005.
- 666 Lehmann, N., Granger, J., Kienast, M., Brown, K. S., Rafter, P. A., Martínez-Méndez, G. and  
667 Mohtadi, M.: Isotopic Evidence for the Evolution of Subsurface Nitrate in the Western  
668 Equatorial Pacific, *J. Geophys. Res. Oceans*, doi:10.1002/2017JC013527, 2018.
- 669 Liu, K. K.: Geochemistry of inorganic nitrogen compounds in two marine environments: The  
670 Santa Barbara Basin and the ocean off Peru, University of Southern California, Los Angeles,  
671 1979.
- 672 Liu, K. K., Su, M. J., Hsueh, C. R. and Gong, G. C.: The nitrogen isotopic composition of nitrate  
673 in the Kuroshio Water northeast of Taiwan: Evidence for nitrogen fixation as a source of  
674 isotopically light nitrate, *Mar. Chem.*, 54(3–4), 273–292, doi:10.1016/0304-  
675 4203(96)00034-5, 1996.
- 676 Lourey, M. J., Trull, T. W. and Sigman, D. M.: Sensitivity of delta N-15 of nitrate, surface  
677 suspended and deep sinking particulate nitrogen to seasonal nitrate depletion in the  
678 Southern Ocean, *Glob. Biogeochem. Cycles*, 17(3), doi:10.1029/2002gb001973, 2003.
- 679 Marconi, D., Alexandra Weigand, M., Rafter, P. A., McIlvin, M. R., Forbes, M., Casciotti, K. L.  
680 and Sigman, D. M.: Nitrate isotope distributions on the US GEOTRACES North Atlantic  
681 cross-basin section: Signals of polar nitrate sources and low latitude nitrogen cycling, *Mar.*  
682 *Chem.*, 177, 143–156, doi:10.1016/j.marchem.2015.06.007, 2015.
- 683 Marconi, D., Sigman, D. M., Casciotti, K. L., Campbell, E. C., Alexandra Weigand, M., Fawcett,  
684 S. E., Knapp, A. N., Rafter, P. A., Ward, B. B. and Haug, G. H.: Tropical Dominance of N<sub>2</sub>  
685 Fixation in the North Atlantic Ocean: Tropical Lead of Atlantic N<sub>2</sub> fixation, *Glob.*  
686 *Biogeochem. Cycles*, 31(10), 1608–1623, doi:10.1002/2016GB005613, 2017.
- 687 Mariotti, A., Germon, J. C., Hubert, P., Kaiser, P., Letolle, R., Tardieux, A. and Tardieux, P.:  
688 Experimental determination of nitrogen kinetic isotope fractionation—some principles—  
689 illustration for the denitrification and nitrification processes, *Plant Soil*, 62(3), 413–430,  
690 1981.
- 691 Marquardt, D. W.: An Algorithm for Least-Squares Estimation of Nonlinear Parameters, *J.*  
692 *Soc. Ind. Appl. Math.*, 11(2), 431–441, doi:10.1137/0111030, 1963.
- 693 Martin, T. S. and Casciotti, K. L.: Paired N and O isotopic analysis of nitrate and nitrite in the  
694 Arabian Sea oxygen deficient zone, *Deep Sea Res. Part Oceanogr. Res. Pap.*, 121, 121–131,  
695 doi:10.1016/j.dsr.2017.01.002, 2017.
- 696 Miyake, Y. and Wada, E.: The Abundance Ratio of <sup>15</sup>N/<sup>14</sup>N in Marine Environments, *Rec.*  
697 *Oceanogr. Works Jpn.*, 9(1), 1967.

698 Palter, J. B., Sarmiento, J. L., Gnanadesikan, A., Simeon, J. and Slater, R. D.: Fueling export  
699 production: nutrient return pathways from the deep ocean and their dependence on the  
700 Meridional Overturning Circulation, *Biogeosciences*, 7(11), 3549–3568, doi:10.5194/bg-7-  
701 3549-2010, 2010.

702 Pantoja, S., Repeta, D. J., Sachs, J. P. and Sigman, D. M.: Stable isotope constraints on the  
703 nitrogen cycle of the Mediterranean Sea water column, *Deep-Sea Res. Part -Oceanogr. Res.*  
704 *Pap.*, 49(9), 1609–1621, doi:10.1016/s0967-0637(02)00066-3, 2002.

705 Peters, B. D., Lam, P. J. and Casciotti, K. L.: Nitrogen and oxygen isotope measurements of  
706 nitrate along the US GEOTRACES Eastern Pacific Zonal Transect (GP16) yield insights into  
707 nitrate supply, remineralization, and water mass transport, *Mar. Chem.*,  
708 doi:10.1016/j.marchem.2017.09.009, 2017.

709 Rafter, P. A. and Charles, C. D.: Pleistocene equatorial Pacific dynamics inferred from the  
710 zonal asymmetry in sedimentary nitrogen isotopes, *Paleoceanography*, 27,  
711 doi:10.1029/2012pa002367, 2012.

712 Rafter, P. A. and Sigman, D. M.: Spatial distribution and temporal variation of nitrate  
713 nitrogen and oxygen isotopes in the upper equatorial Pacific Ocean, *Limnol. Oceanogr.*,  
714 61(1), 14–31, doi:10.1002/lno.10152, 2016.

715 Rafter, P. A., Sigman, D. M., Charles, C. D., Kaiser, J. and Haug, G. H.: Subsurface tropical  
716 Pacific nitrogen isotopic composition of nitrate: Biogeochemical signals and their transport,  
717 *Glob. Biogeochem. Cycles*, 26, doi:10.1029/2010gb003979, 2012.

718 Rafter, P. A., DiFiore, P. J. and Sigman, D. M.: Coupled nitrate nitrogen and oxygen isotopes  
719 and organic matter remineralization in the Southern and Pacific Oceans, *J. Geophys. Res.*  
720 *Oceans*, 118, 1–14, doi:10.1002/jgrc.20316, 2013.

721 Ren, H., Sigman, D. M., Meckler, A. N., Plessen, B., Robinson, R. S., Rosenthal, Y. and Haug, G.  
722 H.: Foraminiferal Isotope Evidence of Reduced Nitrogen Fixation in the Ice Age Atlantic  
723 Ocean, *Science*, 323(5911), 244–248, doi:10.1126/science.1165787, 2009.

724 Ren, H., Chen, Y.-C., Wang, X. T., Wong, G. T. F., Cohen, A. L., DeCarlo, T. M., Weigand, M. A.,  
725 Mii, H.-S. and Sigman, D. M.: 21st-century rise in anthropogenic nitrogen deposition on a  
726 remote coral reef, *Science*, 356(6339), 749–752, doi:10.1126/science.aal3869, 2017.

727 Robinson, R. S., Brunelle, B. G. and Sigman, D. M.: Revisiting nutrient utilization in the glacial  
728 Antarctic: Evidence from a new method for diatom-bound N isotopic analysis,  
729 *Paleoceanography*, 19(3), doi:10.1029/2003pa000996, 2004.

730 Robinson, R. S., Kienast, M., Albuquerque, A. L., Altabet, M., Contreras, S., Holz, R. D., Dubois,  
731 N., Francois, R., Galbraith, E., Hsu, T. C., Ivanochko, T., Jaccard, S., Kao, S. J., Kiefer, T., Kienast,  
732 S., Lehmann, M. F., Martinez, P., McCarthy, M., Mobius, J., Pedersen, T., Quan, T. M.,  
733 Ryabenko, E., Schmittner, A., Schneider, R., Schneider-Mor, A., Shigemitsu, M., Sinclair, D.,

- 734 Somes, C., Studer, A., Thunell, R. and Yang, J. Y.: A review of nitrogen isotopic alteration in  
735 marine sediments, *Paleoceanography*, 27, doi:10.1029/2012pa002321, 2012.
- 736 Rumelhart, D. E., Hinton, G. E. and Williams, R. J.: Learning Representations by Back-  
737 Propagating Errors, *Nature*, 323(6088), 533–536, doi:10.1038/323533a0, 1986.
- 738 Ryabenko, E., Kock, A., Bange, H. W., Altabet, M. A. and Wallace, D. W. R.: Contrasting  
739 biogeochemistry of nitrogen in the Atlantic and Pacific Oxygen Minimum Zones,  
740 *Biogeosciences*, 9(1), 203–215, doi:10.5194/bg-9-203-2012, 2012.
- 741 Sachs, J. P., Repeta D. J.: Oligotrophy and nitrogen fixation during eastern Mediterranean  
742 sapropel events, *Science*, 286(5449), 2485–2488, 1999.
- 743 Sarmiento, J. L., Gruber, N., Brzezinski, M. A. and Dunne, J. P.: High-latitude controls of  
744 thermocline nutrients and low latitude biological productivity, *Nature*, 427(6969), 56–60,  
745 doi:10.1038/nature02127, 2004.
- 746 Schlitzer, R.: Ocean Data View. [online] Available from: [http://www.awi-](http://www.awi-bremerhaven.de/GEO/ODV)  
747 [bremerhaven.de/GEO/ODV](http://www.awi-bremerhaven.de/GEO/ODV), 2002.
- 748 Schlitzer, R., Anderson, R. F., Dodas, E. M., Lohan, M., Geibert, W., Tagliabue, A., Bowie, A.,  
749 Jeandel, C., Maldonado, M. T., Landing, W. M., Cockwell, D., Abadie, C., Abouchami, W.,  
750 Achterberg, E. P., Agather, A., Aguiar-Islas, A., van Aken, H. M., Andersen, M., Archer, C.,  
751 Auro, M., de Baar, H. J., Baars, O., Baker, A. R., Bakker, K., Basak, C., Baskaran, M., Bates, N. R.,  
752 Bauch, D., van Beek, P., Behrens, M. K., Black, E., Bluhm, K., Bopp, L., Bouman, H., Bowman,  
753 K., Bown, J., Boyd, P., Boye, M., Boyle, E. A., Branellec, P., Bridgestock, L., Brissebrat, G.,  
754 Browning, T., Bruland, K. W., Brumsack, H.-J., Brzezinski, M., Buck, C. S., Buck, K. N.,  
755 Buesseler, K., Bull, A., Butler, E., Cai, P., Mor, P. C., Cardinal, D., Carlson, C., Carrasco, G.,  
756 Casacuberta, N., Casciotti, K. L., Castrillejo, M., Chamizo, E., Chance, R., Charette, M. A.,  
757 Chaves, J. E., Cheng, H., Chever, F., Christl, M., Church, T. M., Closset, I., Colman, A., Conway,  
758 T. M., Cossa, D., Croot, P., Cullen, J. T., Cutter, G. A., Daniels, C., Dehairs, F., Deng, F., Dieu, H.  
759 T., Duggan, B., Dulaquais, G., Dumousseaud, C., Echegoyen-Sanz, Y., Edwards, R. L., Ellwood,  
760 M., Fahrbach, E., Fitzsimmons, J. N., Russell Flegal, A., Fleisher, M. Q., van de Flierdt, T.,  
761 Frank, M., Friedrich, J., Fripiat, F., Fröllje, H., Galer, S. J. G., Gamo, T., Ganeshram, R. S., Garcia-  
762 Orellana, J., Garcia-Solsona, E., Gault-Ringold, M., et al.: The GEOTRACES Intermediate Data  
763 Product 2017, *Chem. Geol.*, doi:10.1016/j.chemgeo.2018.05.040, 2018.
- 764 Sigman, D. M. and Casciotti, K. L.: Nitrogen Isotopes in the Ocean, in *Encyclopedia of Ocean*  
765 *Science*, pp. 1884–1894, Academic Press., 2001.
- 766 Sigman, D. M., Altabet, M. A., McCorkle, D. C., Francois, R. and Fischer, G.: The delta N-15 of  
767 nitrate in the Southern Ocean: Consumption of nitrate in surface waters, *Glob. Biogeochem.*  
768 *Cycles*, 13(4), 1149–1166, 1999a.
- 769 Sigman, D. M., Altabet, M. A., Francois, R., McCorkle, D. C. and Gaillard, J. F.: The isotopic  
770 composition of diatom-bound nitrogen in Southern Ocean sediments, *Paleoceanography*,  
771 14(2), 118–134, 1999b.

772 Sigman, D. M., Granger, J., DiFiore, P. J., Lehmann, M. M., Ho, R., Cane, G. and van Geen, A.:  
773 Coupled nitrogen and oxygen isotope measurements of nitrate along the eastern North  
774 Pacific margin, *Glob. Biogeochem. Cycles*, 19(4), doi:10.1029/2005gb002458, 2005.

775 Sigman, D. M., DiFiore, P. J., Hain, M. P., Deutsch, C. and Karl, D. M.: Sinking organic matter  
776 spreads the nitrogen isotope signal of pelagic denitrification in the North Pacific, *Geophys.*  
777 *Res. Lett.*, 36, doi:10.1029/2008gl035784, 2009a.

778 Sigman, D. M., DiFiore, P. J., Hain, M. P., Deutsch, C., Wang, Y., Karl, D. M., Knapp, A. N.,  
779 Lehmann, M. F. and Pantoja, S.: The dual isotopes of deep nitrate as a constraint on the  
780 cycle and budget of oceanic fixed nitrogen, *Deep-Sea Res. Part -Oceanogr. Res. Pap.*, 56(9),  
781 1419–1439, doi:10.1016/j.dsr.2009.04.007, 2009b.

782 Smart, S. M., Fawcett, S. E., Thomalla, S. J., Weigand, M. A., Reason, C. J. C. and Sigman, D. M.:  
783 Isotopic evidence for nitrification in the Antarctic winter mixed layer, *Glob. Biogeochem.*  
784 *Cycles*, 29(4), 427–445, doi:10.1002/2014GB005013, 2015.

785 Somes, C. J., Schmittner, A. and Altabet, M. A.: Nitrogen isotope simulations show the  
786 importance of atmospheric iron deposition for nitrogen fixation across the Pacific Ocean,  
787 *Geophys. Res. Lett.*, 37, doi:10.1029/2010gl044537, 2010.

788 Tawa, A., Ishihara, T., Uematsu, Y., Ono, T. and Ohshimo, S.: Evidence of westward  
789 transoceanic migration of Pacific bluefin tuna in the Sea of Japan based on stable isotope  
790 analysis, *Mar. Biol.*, 164(4), doi:10.1007/s00227-017-3127-8, 2017.

791 Thimm, G. and Fiesler, E.: Optimal Setting of Weights, Learning Rate, and Gain, , 15, 1997.

792 Thunell, R. C., Sigman, D. M., Muller-Karger, F., Astor, Y. and Varela, R.: Nitrogen isotope  
793 dynamics of the Cariaco Basin, Venezuela, *Glob. Biogeochem. Cycles*, 18(3),  
794 doi:10.1029/2003gb002185, 2004.

795 Toggweiler, J. R. and Carson, S.: What Are Upwelling Systems Contributing to the Ocean's  
796 Carbon and Nutrient Budgets?, in *Upwelling in the Ocean: Modern Processes and Ancient*  
797 *Records*, edited by K.-C. . meis C.P. Summerhayes M. V. Angel, R. L. Smith, and B. Zeiischcl,  
798 John Wiley & Sons Ltd., 1995.

799 Toggweiler, J. R., Dixon, K. and Broecker, W. S.: The Peru upwelling and the ventilation of  
800 the South-Pacific thermocline, *J. Geophys. Res.-Oceans*, 96(C11), 20467–20497,  
801 doi:10.1029/91jc02063, 1991.

802 Trull, T. W., Davies, D. and Casciotti, K.: Insights into nutrient assimilation and export in  
803 naturally iron-fertilized waters of the Southern Ocean from nitrogen, carbon and oxygen  
804 isotopes, *Deep Sea Res. Part II Top. Stud. Oceanogr.*, 55(5–7), 820–840,  
805 doi:10.1016/j.dsr2.2007.12.035, 2008.

806 Tuerena, R. E., Ganeshram, R. S., Geibert, W., Fallick, A. E., Dougans, J., Tait, A., Henley, S. F.  
807 and Woodward, E. M. S.: Nutrient cycling in the Atlantic basin: The evolution of nitrate

- 808 isotope signatures in water masses, *Glob. Biogeochem. Cycles*, 29(10), 1830–1844,  
809 doi:10.1002/2015GB005164, 2015.
- 810 Umezawa, Y., Yamaguchi, A., Ishizaka, J., Hasegawa, T., Yoshimizu, C., Tayasu, I., Yoshimura,  
811 H., Morii, Y., Aoshima, T. and Yamawaki, N.: Seasonal shifts in the contributions of the  
812 Changjiang River and the Kuroshio Current to nitrate dynamics in the continental shelf of  
813 the northern East China Sea based on a nitrate dual isotopic composition approach,  
814 *Biogeosciences*, 11(4), 1297–1317, doi:10.5194/bg-11-1297-2014, 2014.
- 815 Voss, M.: Räumliche und zeitliche Verteilung stabiler Isotope (d15N, d13C) in  
816 suspendierten und sedimentierten Partikeln im Nördlichen Nordatlantik, Christian-  
817 Albrechts-Universität zu Kiel., 1991.
- 818 Voss, M., Dippner, J. W. and Montoya, J. P.: Nitrogen isotope patterns in the oxygen-deficient  
819 waters of the Eastern Tropical North Pacific Ocean, *Deep-Sea Res. Part -Oceanogr. Res. Pap.*,  
820 48(8), 1905–1921, doi:10.1016/s0967-0637(00)00110-2, 2001.
- 821 Wada, E.: Nitrogen Isotope Fractionation and Its Significance in Biogeochemical Processes  
822 Occurring in Marine Environments, in *Isotope Marine Chemistry*, pp. 375–398., 1980.
- 823 Wada, E. and Hattori, A.: Nitrogen isotope effects in the assimilation of inorganic  
824 nitrogenous compounds by marine diatoms, *Geomicrobiol. J.*, 1(1), 85–101, 1978.
- 825 Weigend, A. S., Huberman, B. A. and Rumelhart, D. E.: Predicting The Future: A  
826 Connectionist Approach, *Int. J. Neural Syst.*, 1(3), 193–209,  
827 doi:10.1142/s0129065790000102, 1990.
- 828 Wong, G. T. F., Chung, S.-W., Shiah, F.-K., Chen, C.-C., Wen, L.-S. and Liu, K.-K.: Nitrate  
829 anomaly in the upper nutricline in the northern South China Sea - Evidence for nitrogen  
830 fixation, *Geophys. Res. Lett.*, 29(23), 12-1-12-4, doi:10.1029/2002GL015796, 2002.
- 831 Wu, J., Calvert, S. E. and Wong, C. S.: Nitrogen isotope variations in the subarctic northeast  
832 Pacific: relationships to nitrate utilization and trophic structure, *Deep Sea Res. Part*  
833 *Oceanogr. Res. Pap.*, 44(2), 287–314, 1997.
- 834 Yang, S. and Gruber, N.: The anthropogenic perturbation of the marine nitrogen cycle by  
835 atmospheric deposition: Nitrogen cycle feedbacks and the <sup>15</sup>N Haber-Bosch effect, *Glob.*  
836 *Biogeochem. Cycles*, 30(10), 1418–1440, doi:10.1002/2016GB005421, 2016.
- 837 Yang, S., Gruber, N., Long, M. C. and Vogt, M.: ENSO-Driven Variability of Denitrification and  
838 Suboxia in the Eastern Tropical Pacific Ocean, *Glob. Biogeochem. Cycles*, 31(10), 1470–  
839 1487, doi:10.1002/2016GB005596, 2017.
- 840 Yoshikawa, C., Nakatsuka, T. and Wakatsuchi, M.: Distribution of N\* in the Sea of Okhotsk  
841 and its use as a biogeochemical tracer of the Okhotsk Sea Intermediate Water formation  
842 process, *J. Mar. Syst.*, 63(1–2), 49–62, doi:10.1016/j.jmarsys.2006.05.008, 2006.

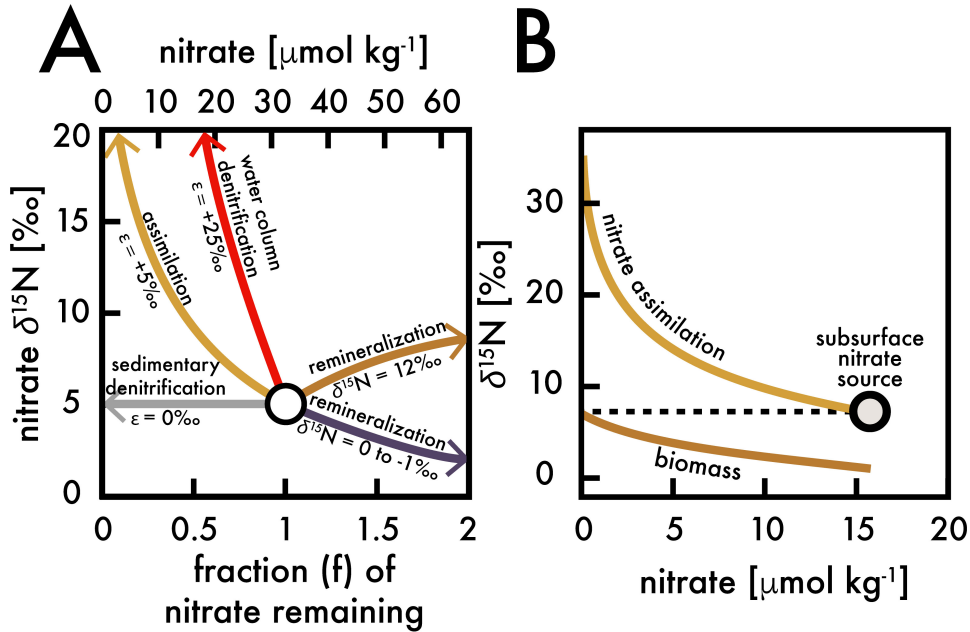
843 Yoshikawa, C., Makabe, A., Shiozaki, T., Toyoda, S., Yoshida, O., Furuya, K. and Yoshida, N.:  
844 Nitrogen isotope ratios of nitrate and N\* anomalies in the subtropical South Pacific,  
845 *Geochem. Geophys. Geosystems*, 16(5), 1439–1448, doi:10.1002/2014GC005678, 2015.

846

**Table 1: Average EANN nitrate  $\delta^{15}\text{N} \geq 3000$  m for each ocean region (tropical being between 23.5° N and 23.5° S)**

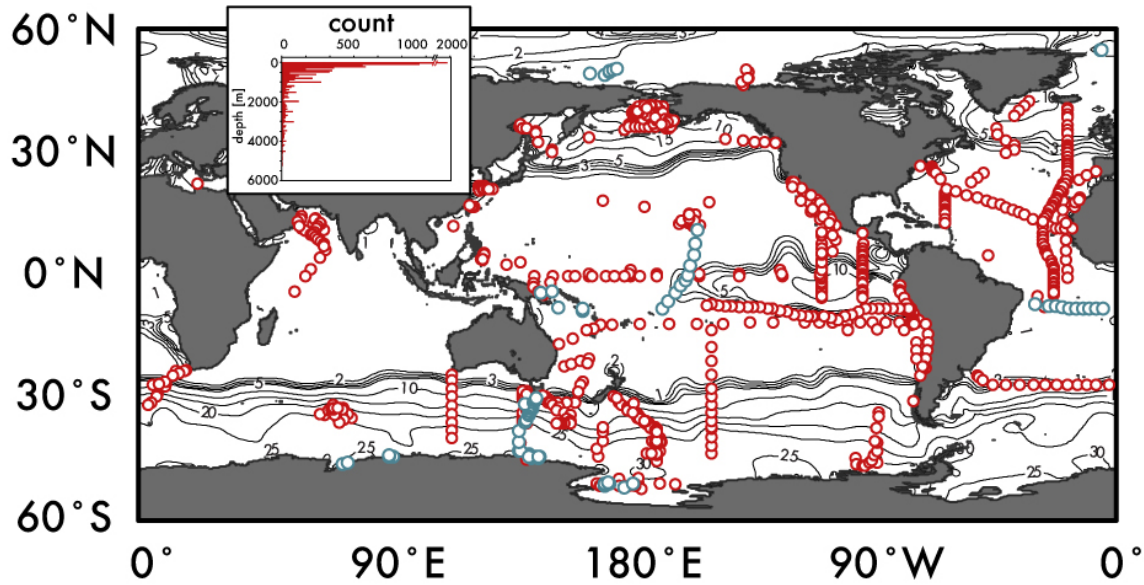
	Indian	Pacific	Atlantic
North	--	5.4±0.2	4.8±0.1
Tropical	5.1±0.2	5.2±0.2	4.9±0.1
South	4.8±0.1	5.0±0.2	4.8±0.1
	Southern	Global	
	4.8±0.1	5.0±0.3	

847

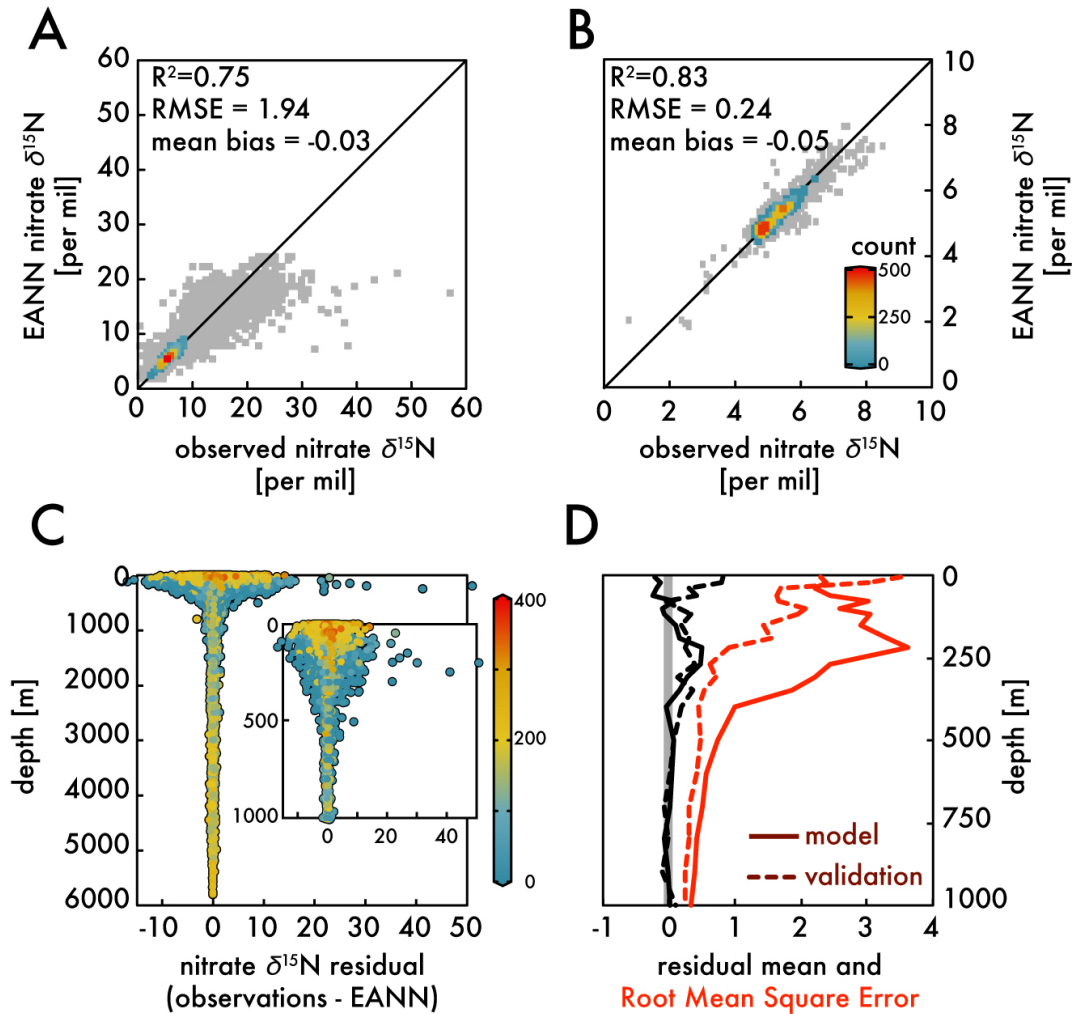


848  
 849 **Figure 1:** (A) A comparison of influences on average deep-sea nitrate (circle; concentration  
 850 and  $\delta^{15}\text{N}$  estimated here by EANN results in this work) including: the isotope effects of  
 851 assimilation (yellow arrow), water column and sedimentary denitrification (red and gray  
 852 arrows), and the addition of nitrate via remineralization of organic matter with higher and  
 853 lower  $\delta^{15}\text{N}$  (brown and purple arrows) (modified from Galbraith et al., (2008)). (B) An  
 854 example of N isotopic fractionation on nitrate and organic matter biomass during nitrate  
 855 assimilation in eastern equatorial Pacific surface waters (from Rafter and Sigman, (2016)).  
 856 These calculations are based on isotopic fractionation equations of (Mariotti et al., 1981)  
 857 simplified in (Sigman and Casciotti, 2001) with an isotope effect ( $\epsilon$ ) as shown in (A). The  
 858 variable “ $f$ ” is the observed / initial nitrate concentration.  
 859  
 860





861  
 862 **Figure 2:** The location of global nitrate  $\delta^{15}\text{N}$  observations used to constrain the Ensemble  
 863 of Artificial Neural Networks are shown as red circles. Observations used as an 'external  
 864 validation dataset' (those withheld from training the EANN) are shown in blue. Inset figure  
 865 shows the number of observations versus depth. Contours are surface nitrate  
 866 concentrations for October-December from World Ocean Atlas (Garcia et al., 2014).  
 867  
 868



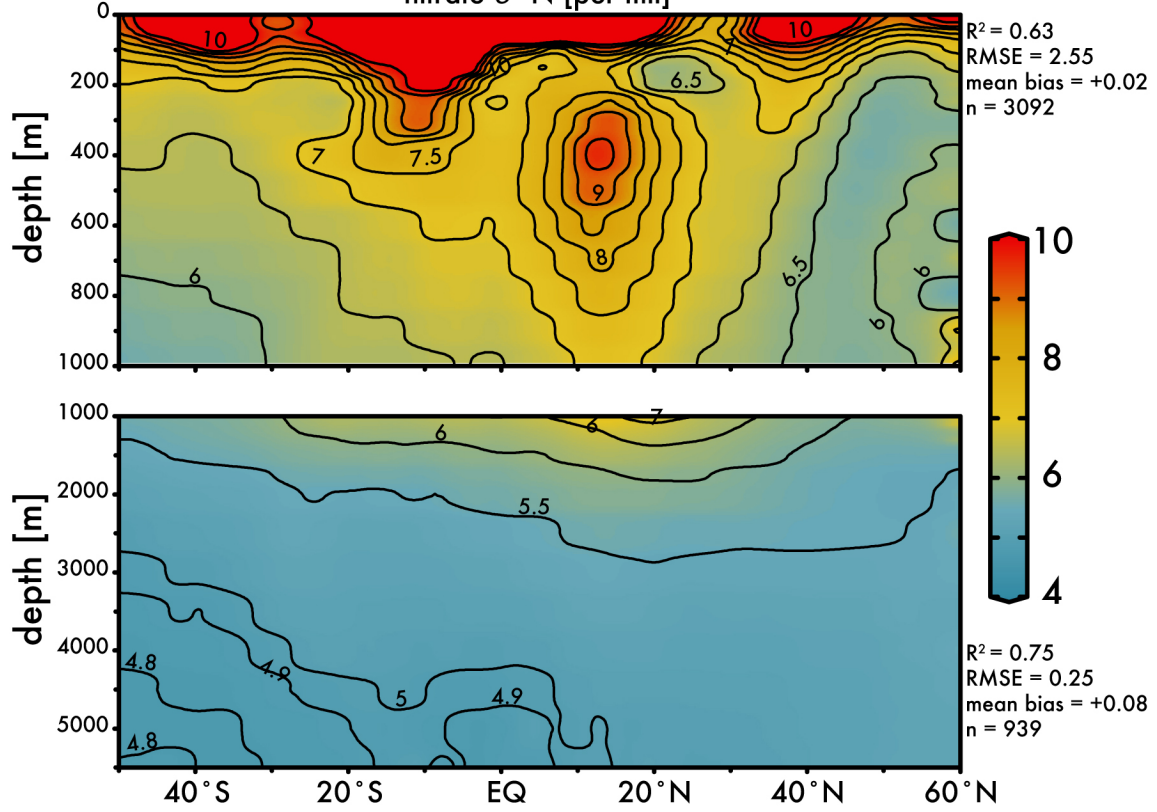
869  
870  
871  
872  
873  
874  
875  
876  
877  
878  
879  
880  
881

**Figure 3:** The binned observed versus EANN-predicted nitrate  $\delta^{15}\text{N}$  are shown for all data at all depths in (A) and for >1000 m in (B). The colors indicate the number of comparisons on the World Ocean Atlas grid. The anomalously high observed nitrate  $\delta^{15}\text{N}$  values (>30‰) in (A) are exclusively from the Eastern Tropical South Pacific waters (Bourbonnais et al., 2015; Casciotti et al., 2013; Rafter et al., 2012; Ryabenko et al., 2012). The difference (or residual) between the observations and EANN nitrate  $\delta^{15}\text{N}$  is made for all depths and the upper 1000 m in (C) with colors representing the dissolved oxygen content. Note the largest offsets between 100-500 m in (C) are associated with lowest oxygen content. Similarly, the mean residual (black) and Root Mean Square Error (RMSE; red) with depth (D) are highest in the upper 500 m. Dashed lines in (D) demonstrate the same statistics, but for the external validation dataset (blue in Fig. 2).

**A**

# Pacific Ocean

nitrate  $\delta^{15}\text{N}$  [per mil]

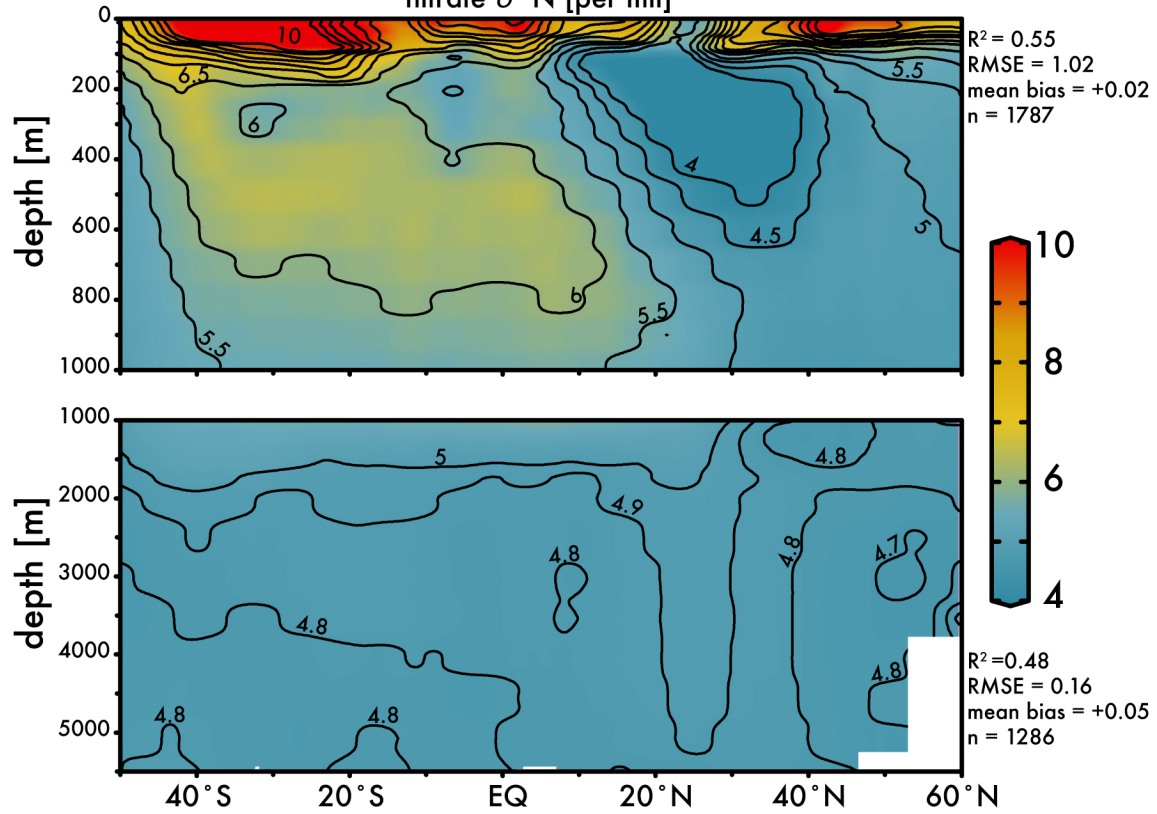


882

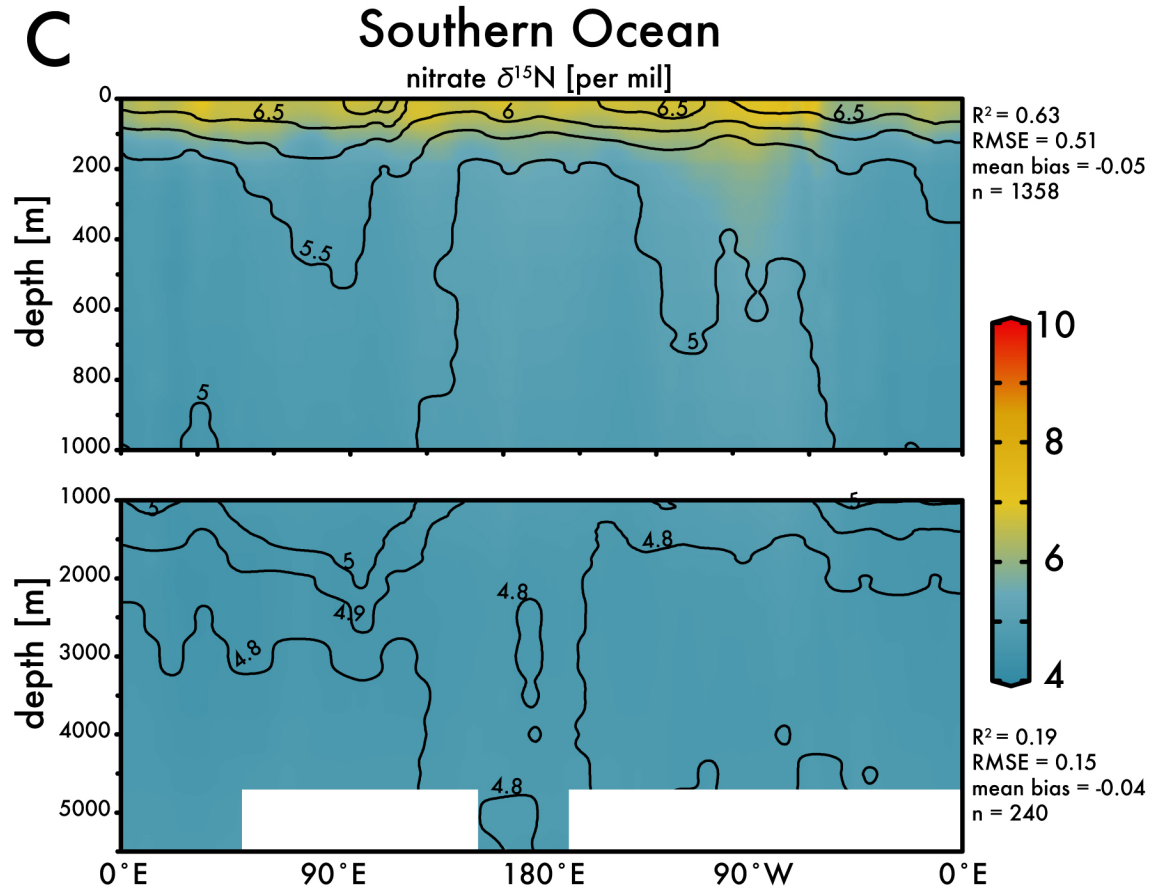
**B**

# Atlantic Ocean

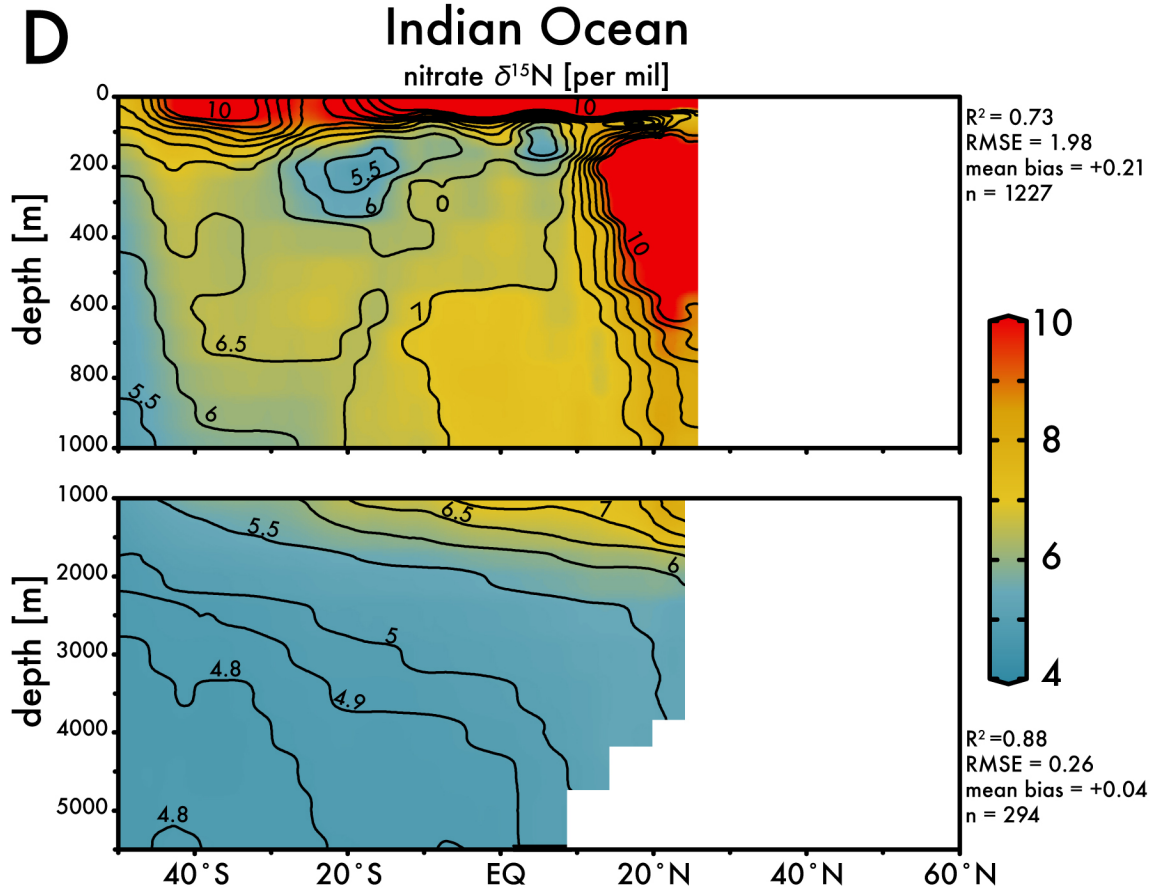
nitrate  $\delta^{15}\text{N}$  [per mil]



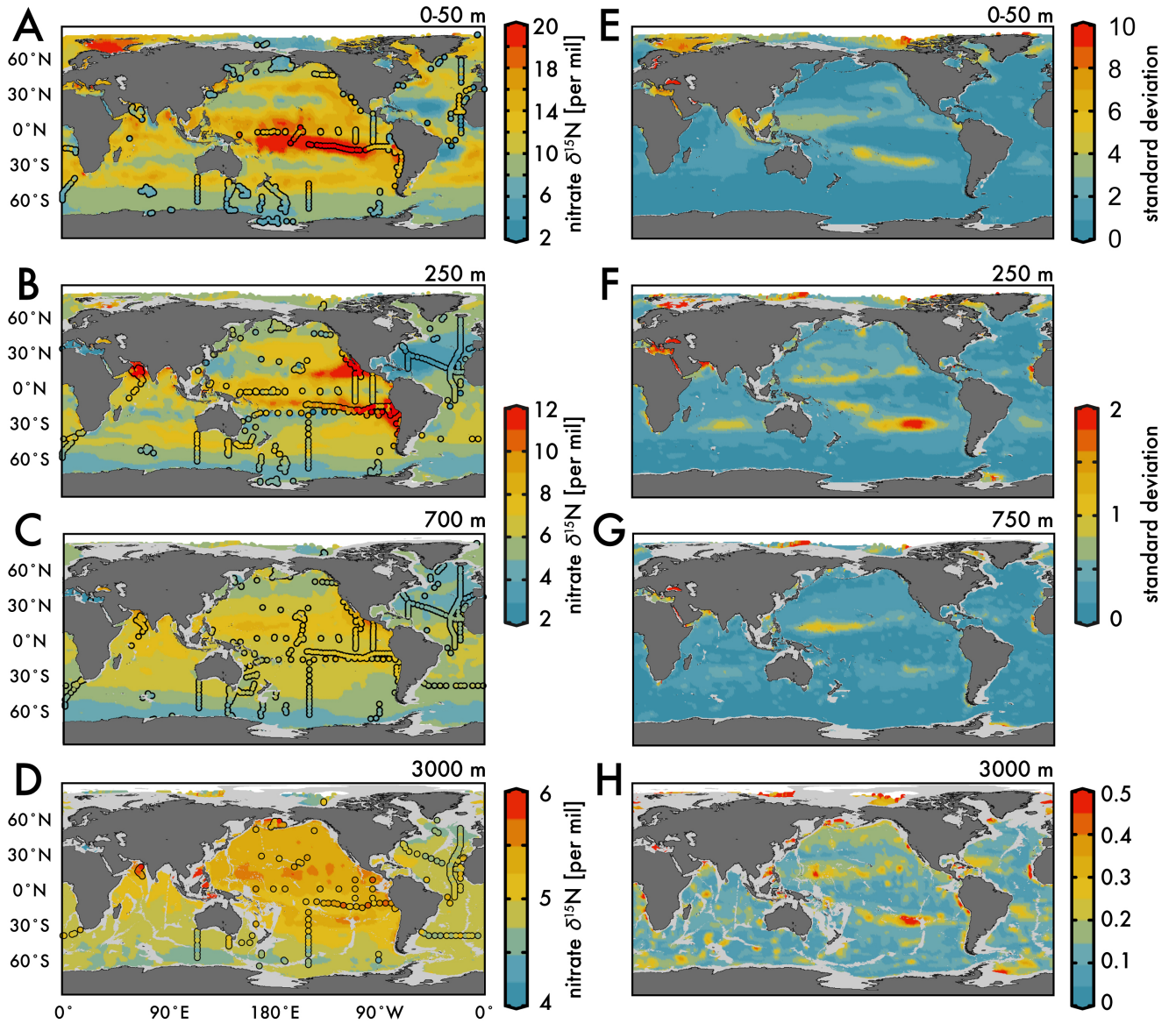
883



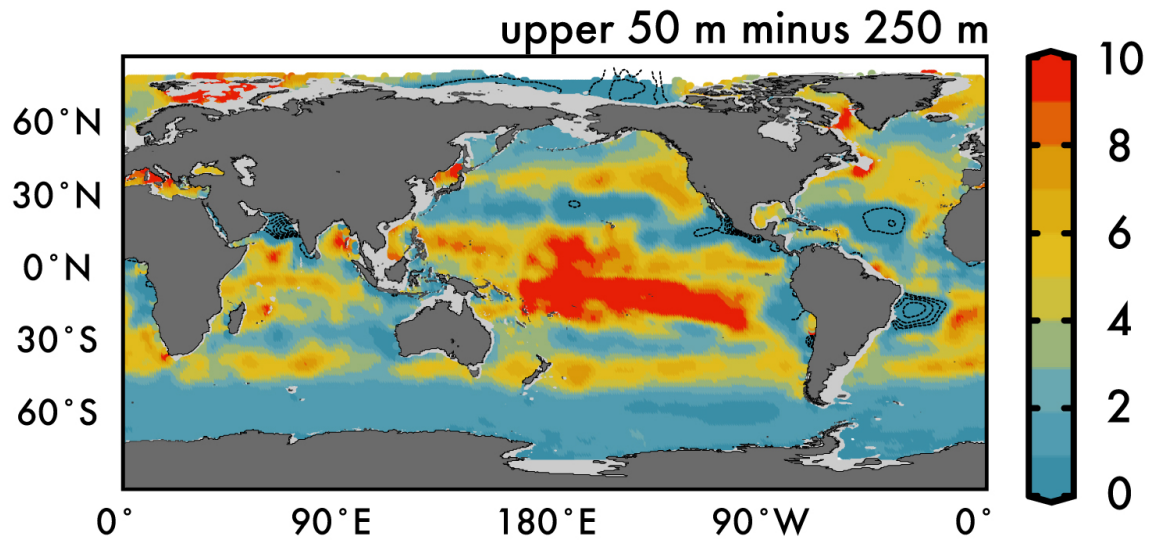
884  
885



886  
887 **Figure 4:** Zonal average of model nitrate  $\delta^{15}\text{N}$  versus latitude or longitude for the: (A)  
888 Pacific Ocean, (B) Atlantic Ocean, (C) Southern Ocean, and the (D) Indian Ocean. White bars  
889 indicate no data because of land. The  $R^2$ , RMSE, mean bias, and total number (n) of  
890 observed versus EANN nitrate  $\delta^{15}\text{N}$  are shown on the right for each region and depth range.  
891 White indicates regions of no data coverage. Note that these zonally-averaged views  
892 obscure zonal gradients in nitrate  $\delta^{15}\text{N}$  (see Figure 5).  
893

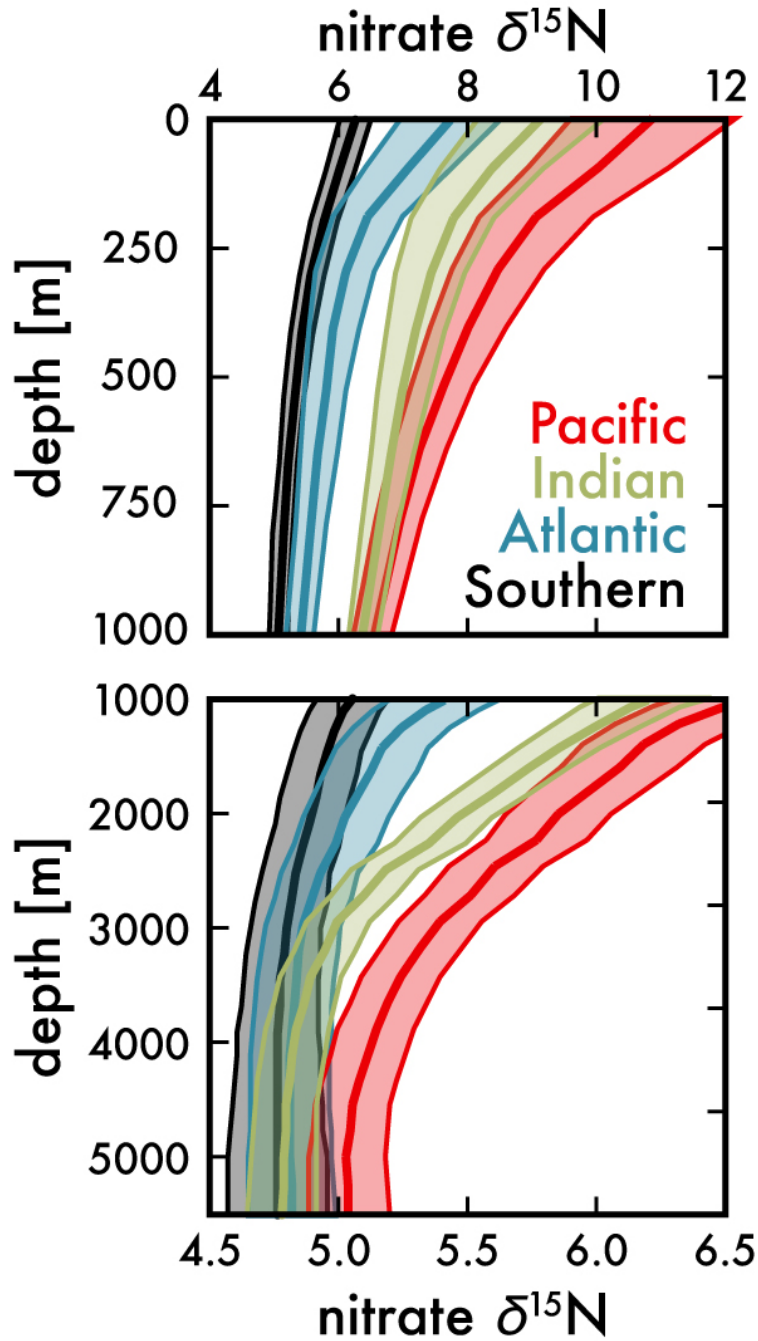


894  
 895 **Figure 5:** (Left) Map view of nitrate  $\delta^{15}\text{N}$  from our EANN and our observations (circles) for  
 896 the (A) average over the 0-50 m depth as well as the (B) 250 m, (C) 700 m, and (D) 3000  
 897 depth surfaces. (Right) Map views of nitrate  $\delta^{15}\text{N}$  error from the EANN model nitrate  $\delta^{15}\text{N}$   
 898 for the same depth surfaces on left.  
 899



900  
 901 **Figure 6:** Difference between the average nitrate  $\delta^{15}\text{N}$  in the upper 50m and 250 m depths  
 902 in Figure 5. Dashed contours in low latitude ODZ regions and subtropical gyres indicate  
 903 regions where nitrate  $\delta^{15}\text{N}$  at 250 m is greater than the upper 50 m nitrate  $\delta^{15}\text{N}$ .  
 904





905  
 906  
 907  
 908

**Figure 7:** Mean EANN nitrate  $\delta^{15}\text{N}$  (solid line) and 1-sigma standard deviation (envelope) with depth for each ocean basin. Note change in vertical and horizontal axes between top and bottom.